PCCP

Accepted Manuscript

ROYAL SOCIETY OF CHEMISTRY

www.rsc.org/pccp

Submit to Physical Chemistry and Chemical Physics

Rotationally resolved state-to-state photoionization and photoelectron study of vanadium monocarbide and its cation (VC/VC$^+$)

Yih Chung Chang[1], Zhihong Luo[1], Yi Pan[2], Zheng Zhang[1], Ying-Nan Song[1], Sophie Yajin Kuang[1], Qing Zhu. Yin[3], Kai-Chung Lau[2,a)] and C. Y. Ng[1,a)]

[1]*Department of Chemistry, University of California, Davis, CA 95616, USA*
[2]*Department of Biology and Chemistry, City University of Hong Kong, 80 Tat Chee Avenue, Kowloon, Hong Kong*
[3]*Department of Earth and Planetary Science, University of California, Davis, CA 95616, USA*

Abstract:

By employing two-color visible (VIS)-ultraviolet (UV) laser photoionization and pulsed field ionization-photoelectron (PFI-PE) techniques, we have obtained highly rotationally resolved photoelectron spectra for vanadium monocarbide cation (VC^+). The state-to-state VIS-UV-PFI-PE spectra thus obtained allow unambiguous assignments for the photoionization rotational transitions, resulting in a highly precise value for the adiabatic ionization energy (IE) of vanadium monocarbide (VC), IE(VC) = 57,512.0 ± 0.8 cm^{-1} (7.13058 ± 0.00010 eV), which is defined as the energy of the $VC^+(X^3\Delta_1; v^+ = 0; J^+ = 1) \leftarrow VC(X^2\Delta_{3/2}; v'' = 0; J'' = 3/2)$ photoionization transition. The spectroscopic constants for $VC^+(X^3\Delta_1)$ determined in the present study include the harmonic vibrational frequency ω_e^+ = 896.4 ± 0.8 cm^{-1}, the anharmonicity constant $\omega_e^+x_e^+$ = 5.7 ± 0.8 cm^{-1}, the rotational constants B_e^+ = 0.6338 ± 0.0025 cm^{-1} and α_e^+ = 0.0033 ± 0.0007 cm^{-1}, the equilibrium bond length r_e^+ = 1.6549 ± 0.0003 Å, and the spin-orbit coupling constant A = 75.2 ± 0.8 cm^{-1} for $VC^+(X^3\Delta_{1,2,3})$. These highly precise energetic and spectroscopic data are used to benchmark state-of-the-art CCSDTQ/CBS calculations. In general, good agreement is found between the theoretical predictions and experimental results. The theoretical calculations yield the values, IE(VC) =7.126 eV; the 0 K bond dissociation energies: D_0(V–C) = 4.023 eV and $D_0(V^+–C)$ = 3.663 eV; and heats of formation: ΔH^o_{f0}(VC) =

835.2, $\Delta H^{o}_{f298}(VC) = 840.4$, $\Delta H^{o}_{f0}(VC^{+}) = 1522.8$, and $\Delta H^{o}_{f298}(VC^{+}) = 1528.0$ kJ mol^{-1}.

---

a) To whom correspondence should be addressed. Electronic mails: kaichung@cityu.edu.hk and cyng@ucdavis.edu

1. Introduction

Understanding the chemical bonding between transition metal and main group elements is of interest to many research fields, including organometallic chemistry, catalysis, and astrophysics.[1-5] However, due to the difficulty of preparing transition metal species in the gas phase with a sufficiently high intensity, the determination of accurate 0 K bond energies (D_0) and electronic structures of transition metal-containing molecules in the gas phase, even for the simplest diatomic molecular systems, remains challenging. From the theoretical prospective, it is well known that the partially electron-filled *d*-shell of a transition metal atom (M) can give rise to a significant number of low lying multiplicity states for transition metal-containing molecules and their ions. In order to achieve reliable energetic and spectroscopic predictions for transition metal-containing neutral and ionic species, it is necessary to take into account of extensive electron correlations in *ab initio* quantum chemical calculations.[6] Even for diatomic transition metal carbides, nitrides, and oxides (MX, X = C, N, and O), it remains difficult to obtain accurate theoretical predictions for the term symmetry of the neutral or ionic ground state.

Many experimental and theoretical studies on neutral vanadium monocarbide (VC) have been reported previously.[4,7-13] The ground state symmetry of VC was first reported to be of $^2\Sigma^+$ symmetry by an early matrix isolation electron spin resonance (ESR) study, but was latter reassigned as $^2\Delta_{3/2}$ symmetry based on a subsequent ESR experiment.[7,8] Several theoretical studies have been conducted to investigate the electronic structure and bonding characters of VC, suggesting the possible ground-state term symmetry to be $^2\Delta$ or $^4\Delta$.[9-13] In 2005, a high-level *ab initio* quantum chemical study on VC at the multi-reference configuration interaction (MRCI) level was reported by Kalemos *et al*., suggesting that $^2\Delta$ is the ground state for VC.[12] A subsequent high-resolution spectroscopic study of Krechkivska and Morse[4] confirmed the ground electronic state symmetry for VC to be $^2\Delta_{3/2}$, and has provided highly precise values for the rotational constant (B'') and bond length (r_0'') of the VC($X^2\Delta_{3/2}$) ground state in the same study. Thus, the electronic structure for the neutral VC($X^2\Delta_{3/2}$) ground state can be considered as well established.

The present high-resolution photoionization and photoelectron study of the VC/VC^+ system is partially motivated by the lack of precise experimental energetic and spectroscopic data for the VC^+ cation. The overwhelming majority of previous investigations on the VC^+ cation were theoretical in nature. To our knowledge, no spectroscopic measurement on VC^+ is available in the literature. Sixteen electronic states of the VC^+ cation were predicted to situate within 2 eV above its ground state. Three electronic states, $^3\Delta$, $^1\Sigma^+$, and $^1\Delta$, were shown to be good candidates for the ground electronic state of VC^+.[14] On the basis of density functional (DFT) calculations, Gutsev *et al.*[13] have reported energetic and spectroscopic predictions for the $VC^+(X)$ ground state. Their DFT calculations also yielded a IE prediction for VC to be IE(VC) = 7.36 eV.[13] Kerkins and Mavridis have investigated the electronic structures and bonding properties of 17 low-lying electronic states of VC^+ at the MRCI level using large basis sets. This study predicts $^3\Delta$ to be the ground electronic state with the $^1\Sigma^+$ and $^1\Delta$ states to situate at 0.13 and 0.36 eV, respectively, above its ground state.[14] Up to now, the only experimental energetic information available for VC^+ is its 0 K bond dissociation energy (D_0), which was reported[15,16] to be 3.87 ± 0.14 and 3.95 ± 0.04 eV based on two guided ion beam ion-molecule collision studies.

The determination of the term symmetry for the electronic state of VC^+ requires rotationally resolved spectroscopic measurements. The two-color IR-UV and VIS-UV pulsed field ionization-photoelectron (PFI-PE) measurements have been demonstrated to be capable of providing cleanly rotationally resolved state-to-state photoelectron spectra for the cations of many diatomic and triatomic transition metal-containing molecules.[17-24] On the theoretical end, we have demonstrated that the coupled cluster theory with electronic excitations up to quadruple (CCSDTQ) combined with the complete basis set (CBS) technique is capable of giving reliable IE and D_0 predictions for 3*d* transition metal carbides, including FeC/FeC^+, NiC/NiC^+ and CoC/CoC^+,[25-27] the discrepancies between these IE and D_0 predictions and highly precise experimental values were found to be within 30 meV. In this report, we present a high-resolution study of VC^+ by using the VIS-UV-photoionization efficiency (VIS-UV-PIE) and VIS-UV-PFI-PE detection schemes, along with

state-of-the-art CCSDTQ/CBS calculations on the IE, D_0, 0 K and 298 K heats of formation (ΔH^o_{fT}, T = 0 and 298 K) values for the VC/VC^+ system. The rotationally selected and resolved state-to-state PFI-PE spectra thus obtained for VC^+ have allowed the unambiguous determination of the ground-state electronic symmetry as well as highly precise energetic and spectroscopic data, including the IE(VC), harmonic vibrational frequency (ω_e^+), anharmonicity constant ($\omega_e^+ x_e^+$), rotational constants (B_e^+ and α_e^+) and equilibrium bond length (r_e^+), and the spin-orbit coupling constant (A) for $VC^+(X)$. These highly precise energetic and spectroscopic data are valuable for the development of *ab initio* computation procedures for providing more accurate thermochemical and structural predictions for transition metal-containing compounds.

Recently, we have successfully performed a state-to-state IR-UV-PFI-PE study of the vanadium methylidyne cation (VCH^+), providing a highly precise value for the IE(VCH).[17] According to the conservation of energy, the difference between the D_0 value for the V^+–CH bond [D_0 (V^+–CH)] and that for the V–CH bond [D_0(V^+–CH)] can be obtained by the relation: $D_0(V^+–CH) – D_0(V–CH)$ = IE(V) – IE(VCH). Since IE(V) is known[28] and thus the measurement of the IE(VCH) allows the determination of $D_0(V^+–CH) – D_0(V–CH)$. Similarly, we have the relation: $D_0(VC^+–H) – D_0(VC–H)$ = IE(VC) – IE(VCH), which makes possible the determination of the difference $D_0(VC^+–H) – D_0(VC–H)$ by the measurements of both the IE(VC) and the IE(VCH). The ability to perform simultaneous probes on the V–CH and the V–CH bond strengths upon photoionization of VCH requires the determination of IE(VC) as well as IE(VCH). This is also a motivation for the present VIS-UV-PFI-PE study for VC^+.

2. Experimental and theoretical considerations

2.1. Experiment

The apparatus and procedures used in this work are similar to those employed in previous VIS-UV-PFI-PE studies of transition metal-containing molecular systems and have been described in

detail.[18-24] The apparatus consists of a Smalley-type[29] molecular beam laser ablation source for the preparation of cold gaseous VC molecules, two independently tuned dye lasers for photoexcitation and photoionization of the VC sample, a time-of-flight (TOF) mass spectrometer for photoion detection, and a TOF spectrometer for the detection of PFI-PEs.

The gaseous VC molecules were generated by reacting V atoms with CH_4 in a gas mixture of CH_4/He with a ratio of <1%, which were introduced into the reaction channel of the beam source by a pulsed valve (30 Hz) with a total stagnation pressure of 40 psi. The V atoms were produced by laser ablation on a rotating and translating vanadium rod (American Element, 99% purity) by using the second harmonic output (532 nm) of a Nd: YAG laser (Continuum, Surlite-1-30) with a pulse energy of about 2 mJ. The VC molecular sample formed in the reaction channel of the beam source was further cooled by supersonic expansion, and skimmed by a conical skimmer (diameter = 1mm), before entering the photoionization /photoexcitation (PI/PEX) center, where the cold VC beam sample intersects with the dye laser beams for photoexcitation and photoionization.

Two independently tunable dye lasers [Lambda Physik model FL 2002; optical bandwidth = 0.4 cm^{-1}, full-width at half-maximum (FWHM) and Lambda Physik model FL 3002; optical bandwidth = 0.2 cm^{-1} (FWHM)], which were optically pumped by an identical Nd:YAG laser (Spectra-Physics, Quantum-Ray PRO-230, 30 Hz), provide the visible (VIS) ω_1 and the ultraviolet (UV) ω_2 outputs required by the experiment. In PIE measurements, a dc electric field of 18.5 V/cm was applied at the PI/PEX region to extract and guide the photoions toward the TOF mass spectrometer for detection by a dual multichannel plate ion detector. In VIS-UV-PFI-PE measurements, a small pulsed electric field (0.1 V/cm) was applied to the PI/PEX region at a delay of 150 ns with respect to the UV ω_2 pulse to disperse energetic prompt electrons. At a delay of 2 μs with respect to the UV ω_2 pulse, a pulsed electric field of 0.6 V/cm was applied at the PI/PEX region for PFI of high-n (n > 100) Rydberg VC*(n) molecules and for extracting PFI-PEs toward the electron TOF spectrometer for detection by the multichannel plate electron detector. Our

previous studies have shown that it is essential to keep the PI/PEX region field free during the laser excitation to minimize the destruction of high-*n* Rydberg species in order to obtain the best PFI-PE signal.[30,31] All spectra for VC/VC$^+$ presented in this work represent the average of at least three reproducible scans. Unless specified, all energetic values such as IEs, present here have been corrected for the Stark shift induced by the pulsed electric field applied for PFI-PE measurements.[20]

2.2. Theoretical considerations

In the coupled cluster calculations using the CCSDTQ/CBS procedures, we have chosen to use the partially unrestricted implementation, conventionally labeled as ROHF-UCCSD(T). This method is based on restricted open-shell Hartree–Fock (ROHF) orbitals and relaxes the spin restriction throughout the calculations.[32,33]

The CCSDTQ/CBS calculations involve the approximation to the CBS limit at the CCSD(T) level of theory. The ground state structures of the VC($X^2\Delta$) and VC$^+$($X^3\Delta$) have been optimized at the CCSD(T) level, proceeding from aug-cc-pwCVTZ, to aug-cc-pwCVQZ, to aug-cc-pwCV5Z[34,35] basis sets. The geometry optimizations correlate the 1*s*2*s*2*p* electrons on carbon and 3*s*3*p*3*d*4*s* electrons on vanadium. The 1*s*2*s*2*p* electrons on vanadium are kept frozen and uncorrelated. The total CCSD(T) energies are used to extrapolate the energies at the CBS limit ($E_{\text{extrapolated CBS}}$) by the two schemes:

(i) A three-point extrapolation scheme[36] using the mixed exponential/Gaussian function of the form:

$$E(\mathrm{X}) = E_{\text{extrapolated CBS}} + \mathrm{B}\exp[-(\mathrm{X}-1)] + \mathrm{C}\exp[-(\mathrm{X}-1)^2], \quad (1)$$

where X = 3, 4, and 5 represent the use of the aug-cc-pwCVTZ, aug-cc-pwCVQZ, and aug-cc-pwCV5Z basis sets, respectively.

(ii) A two-point extrapolation scheme[37,38] using the simple power function involving the reciprocal of X,

$$E(\mathrm{X}) = E_{\mathrm{extrapolatedCBS}} + \frac{\mathrm{B}}{\mathrm{X}^3}, \quad (2)$$

where X = 4 and 5 represent the use of aug-cc-pwCVQZ and aug-cc-pwCV5Z basis sets, respectively. Previous calculations on FeC/FeC$^+$,[25] NiC/NiC$^+$,[26] CoC/CoC$^+$,[27] and other main-group molecules[39] reveal that the difference of extrapolated energetics between the two-point and three-point extrapolation schemes are typically small, thus the average of the two extrapolated energies are adopted.

The higher-order energy correction (HOC) incorporates higher-order triple and quadruple excitations, where the full triple excitation effect is estimated by the difference between CCSDT and CCSD(T) energies and the iterative quadruple excitations are estimated as the difference of CCSDTQ and CCSDT energies. The HOC for VC/VC$^+$ is taken as:

$$E_{\mathrm{HOC}} = E_{\mathrm{CCSDT/aug-cc-pVQZ}} - E_{\mathrm{CCSD(T)/aug-cc-pVQZ}} + E_{\mathrm{CCSDTQ/cc-pVTZ}} - E_{\mathrm{CCSDT/cc-pVTZ}}, \quad (3)$$

The scalar relativistic (SR) energy is computed using the spin-free, one-electron Douglas-Kroll-Hess (DKH) Hamiltonian.[40,41] The calculations are done with the DKH-contracted aug-cc-pV5Z-DK basis sets[35,42] at the CCSD(T) level. The SR energetic contributions (E_{SR}) are taken as the difference between electronic energies at the CCSD(T)/aug-cc-pV5Z level without using DKH Hamiltonian and at the CCSD(T)/aug-cc-pV5Z-DK level with DKH Hamiltonian. The relativistic effect due to complete triple and quadruple excitations are also included in a similar manner as described in Eq. (3), except that the aug-cc-pVQZ-DK and cc-pVTZ-DK basis sets are used in the respective CCSDT and CCSDTQ calculations.

The electronic correlation contributions between core and valence electrons and those within core electrons have already been included in the single-point energy and geometrical optimization calculations at

the CCSD(T) level. Additional core-valence electronic correlations (E_{CV}) from full triple excitations are obtained as the difference between CCSD(T) and CCSDT energies with the aug-cc-pwCVTZ basis set.[34,35] The core 1*s* electrons on carbon and outer-core 3*s*3*p* electrons on vanadium are correlated.

The molecular spin-orbit coupling (E_{SO}) of VC/VC^+ are computed by first-order perturbation theory. The calculations use the uncontracted aug-cc-pVTZ basis set including the *s*, *p*, *d* and *f* functions on V and the *s*, *p*, *d* functions on C. Spin-orbit matrix elements are computed among the components of the VC/VC^+ states using internally contracted MRCI wavefunctions.[43] The SO calculations of VC and VC^+ have included the lowest two electronic states, which correlate to the asymptotic products of V(^{4}F) + C(^{3}P) and V^+(^{5}D) + C(^{3}P), respectively. The 2*s*2*p* electrons on C and the 3*d*4*s* electrons on V are included in the active space. The atomic spin-orbit correction of V/V^+ are done in a similar manner. The atomic spin-orbit correction (0.37 kJ mol^{-1}) for carbon is directly taken from the experimental excitation energies tabulated by Moore.[44]

In the present work, all the CCSD(T) single-point energy and correlation contribution calculations are performed using the MOLPRO 2010.1 program[45] and the CCSDT/CCSDTQ calculations are done with the string-based many-body MRCC program[46] interfaced with MOLRPO. The harmonic vibrational frequencies calculated at the CCSDTQ/cc-pVTZ level are used for zero-point vibrational energy corrections (ΔE_{ZPVE}). The ω_e (ω_e^+) values at the CCSDT, CCSDTQ and MRCI(+Q) levels are obtained numerically. The ΔH^o_{f0} and ΔH^o_{f298} values for VC and VC^+ were obtained using the atomization scheme[47] and the following experimental thermochemical data[48] (in kJ mol^{-1}): ΔH^o_{f0}(V) = 512.2, ΔH^o_{f298}(V) = 515.5, ΔH^o_{f0}(C) = 711.2, and ΔH^o_{f298}(C) = 716.7. The 298 K thermal and enthalpy corrections to 0 K energies for elements and compounds are estimated using the methods adopted from reference 47.

3. Results and discussion

3.1. Preparation of the intermediate VC* excited state

To conduct state-to-state VIS-UV-PFI-PE measurements for VC^+, it is necessary to first investigate and perform a detailed simulation of a rovibronically resolved excitation transition band of neutral VC in the VIS range, such that excited intermediate VC* molecules thus prepared in single rovibronic levels can be detected by UV photoionization and photoelectron measurements. We have surveyed several rovibronic transition bands of neutral VC by means of the resonance enhanced VIS-UV photoionization scheme covering the VIS ω_1 region of 20,933–21,725 cm^{-1}. The excitation spectrum for the VC* state obtained by scanning VIS ω_1 in the range of 21,639–21,724 cm^{-1} while fixing UV ω_2 at 47,170 cm^{-1} for photoionization detection is depicted as the lower curve in Fig. 1. The upper blue curve of Fig. 1 is the simulated spectrum, which was obtained based on the least square fits of observed rotational transition energies (ν's) to the standard formula of rovibronic transitions:

$$\nu = \nu_{v'0} + B'[J'(J'+1) - \Omega'^2] - B''[J''(J''+1) - \Omega''^2], \quad J'' \geq \Omega'', J' \geq \Omega'. \tag{4}$$

Here $\nu_{v'0}$ represents the origin of the intermediate VC* transition band, $J''(J')$ is the total angular momentum of the VC ground (VC* excited) state, and $\Omega''(\Omega')$ is the projected total angular momentum along the inter-nuclear axis of the VC ground (VC* excited) state. As pointed out above, the high-resolution spectroscopic study of Krechkivska and Morse has confirmed that the ground electronic state of VC is of $^2\Delta_{3/2}$ symmetry with the rotational constant of B'' = 0.66281(28) cm^{-1}.[4] The latter Ω'' and B'' values were adopted directly in the spectral simulation. The simulated spectrum was constructed assuming a Gaussian instrumental line profile (FWHM = 0.4 cm^{-1}) for optical excitation, and the Boltzmann rotational distribution of the VC($X^2\Delta_{3/2}$; v'' = 0) ground state governed by a rotational temperature of 30 K. The simulated spectrum confirms Ω' = 2.5 and the least square fits of the observed rotational photoionization transitions to Eq. (4) yields $\nu_{v'0}$ = 21,716.91 ± 0.03 cm^{-1}, B'= 0.5090 ± 0.0011 cm^{-1}.

Because the vibrational assignment is unfeasible, the present VC* transition band was labeled as the {21.72} Ω' = 2.5 band following the notation used by Krechkivska and Morse.[4] The rotational assignments of the P, Q, and R-branches based on the least square fits are marked on the top of the simulated spectrum of Fig. 1. The transition lines, Q(7.5), P(5.5) and Q(8.5), marked by asterisks in the stimulated spectrum, are missing in experimental spectrum, which are caused by a serious saturation effect of the MCP ion detector, arising from the very intense V^+ ion signal produced by VIS-UV photoionization of V atoms at VIS ω_1 = 21,704.04 cm^{-1}. The latter transition energy can be attributed to the V($3d^3(^4F)4s4p(^3P^0)$ $z^4G^0_{5/2}$) ← V($3d^34s$ $a^4F_{5/2}$) atomic transition.[49] Based on the intensity pattern of rotational transitions, along with identification of Ω' = 2.5, we tentatively assigns the excitation {21.72} Ω'=2.5 band as the formation of the intermediate VC* excited electronic state with the $^2\Phi_{5/2}$ symmetry.

The TOF mass spectrum shown (as the upper spectrum) in Fig. 2 was recorded by means of the VIS-UV photoionization detection by setting VIS ω_1 = 21717.27 cm^{-1} (the most intense peak or the band head of the excitation band) and UV ω_2 = 47169.8 cm^{-1}. The photoionization detection required that the total energy $\omega_1 + \omega_2$ (68887.07 cm^{-1}) is greater than the IE(VC). The lower mass spectrum of Fig. 2 was recorded under the same experimental conditions except that the VIS ω_1 was blocked off. The mass peaks observed at 51, 63 and 67 amu in these mass spectra are assigned as the V^+, VC^+ and VO^+ ion peaks, respectively. The comparison of the upper and lower spectra of Fig. 2 shows that VC^+ ions are only formed by two-color VIS-UV photoionization. The V^+ and VO^+ ion signals, which appear to have nearly the same intensities in both mass spectra, are mainly produced by UV-UV and/or UV-VIS two-photon photoionization.

3.2. VIS-UV-PIE spectrum for VC^+

Figure 3 depicts the VIS-UV-PIE spectrum for VC^+ near the ionization threshold of VC obtained by setting VIS ω_1 = 21717.27 cm^{-1}, and scanning UV ω_2 in the range of 35643.2-37000.0 cm^{-1} (bottom energy scale). Thus, the total energy $\omega_1 + \omega_2$ is in the range of 57360.4-58717.3 cm^{-1} (top energy scale). According

to the simulation of the excitation spectrum of Fig. 1, the setting of VIS ω_1 = 21717.27 cm^{-1} corresponds to R-branch band head, VC* molecules thus formed are expected to populate in the J' = 2.5-5.5 rotational levels from the R(J''), J''= 1.5-4.5, rotational transitions of the VC($X^2\Delta_{3/2}$, v" = 0) ground state. The VIS-UV-PIE spectrum for VC^+ of Fig. 3 was severely modulated by sharp and intense transition resonances of V atom. Similar observation was found in the previous VIS-UV-PIE studies of NiC and CoC.[19,20]

Although the VIS-UV-PIE spectrum of Fig. 3 suffers from intense modulation due to atomic V transition resonances, a sharp step-like onset is still observable at $\omega_1+ \omega_2$ = 57,497.6 cm^{-1} (marked by downward pointing arrow). The VC^+ ion signal below this PIE onset is in the noise level, suggesting that the position of this step can be identified as the adiabatic IE(VC). After taking into account of the Stark shift induced by the dc electric field of 18.5 V/cm applied at the PI/PEX for PIE measurements, we obtained the IE(VC) = 57,511 ± 6 cm^{-1}. A second PIE step is also evident at $\omega_1+ \omega_2$ = 58,398.2 cm^{-1} (marked by dropped line in Fig. 3), which can be assigned as the ionization onset for the photoionization transition $VC^+(X; v^+=1) \leftarrow VC(X^2\Delta_{3/2}; v'' = 0)$. After correcting for the Stark shift, the IE for the formation of $VC^+(X; v^+ = 1)$ is determined to be 58,415 ± 6 cm^{-1}.

From the molecular-orbital point of view, the ground electronic state of VC has an $^2\Delta$ symmetry, arising from the CASSCF dominant electronic configuration of $0.90|(7\sigma)^2(3\pi)^4(8\sigma)^2(1\delta)^1>$. The valence electrons of VC are contributed by the $4s^23d^3$ electrons of V and the $2s^22p^2$ electrons of C. The 7σ orbital is dominated by the C(2*s*) character. Assuming that the VC molecule lies along the *z*-axis, the 8σ orbital is formed by the overlap of the V($3d_z^2$) and C($2p_z$) orbitals, with the former one being dominant in contribution. The two degenerate π bonding orbitals, $3\pi_x$ and $3\pi_y$, are formed by the overlaps of V($3d_{xz}$) with C($2p_x$) and V($3d_{yz}$) with C($2p_y$), respectively; the 2*p* orbital of C has an even contribution in both orbitals. The 1δ orbital is consisting of the V($3d_{x^2-y^2}$) or V($3d_{xy}$) orbital. On the basis of the Mulliken atomic distribution, the VC($X^2\Delta$) has a triple bond, consisting of two π ($3\pi^4$) and one σ ($8\sigma^2$) bonds. The first

ionization of VC($X^2\Delta$) involves the ejection of the electron occupying the 8σ orbital, resulting in a $^3\Delta$ ground state in $VC^+(X^3\Delta)$ and its CASSCF electronic configuration is: $0.89|(7\sigma)^2(3\pi)^4(8\sigma)^1(1\delta)^1>$.

3.3. VIS-UV-PFI-PE spectra for $VC^+(X^3\Delta_{1,2,3}; v^+ = 0)$

The VIS-VU-PIE spectrum of Fig. 3 was useful for narrowing the total energy $\omega_1 + \omega_2$ range in VIS-UV-PFI-PE measurements for the $VC^+(X^3\Delta; v^+ = 0, 1)$ states. Figures 4(a), 4(b), 4(c), and 4(d) depict the rotationally selected and resolved state-to-state VIS-UV-PFI-PE spectra for the formation of $VC^+(X^3\Delta; v^+ = 0, J^+)$ obtained by setting the VIS ω_1 at the respective Q(2.5), Q(3.5), Q(4.5), and Q(5.5) transitions of Fig. 1 and measuring the PFI-PEs intensity in the UV ω_2 range of 35744.48-35834.16 cm^{-1}. For all figures showing the VIS-UV-PFI-PE spectra here, such as those of Figs. 4(a)-4(b), the top horizontal axis of the figures represents the total energy $\omega_1 + \omega_2$ scale, while the bottom horizontal axis represents the UV ω_2 scale.

The observation of the VIS-UV-PFI-PE spectra in the vicinity of the first VIS-UV-PIE onset for VC^+ supports that the PFI-PE signal is resulted from photoionization of VC molecules. Since the VIS ω_1 excitation of the Q(2.5), Q(3.5), Q(4.5), and Q(5.5) transitions is expected to populate VC molecules in single rotational levels VC*(J'), $J' = 2.5$, $J' = 3.5$, $J' = 4.5$ and $J' = 5.5$, respectively, each J^+ rotationally resolved peak in the VIS-UV-PFI-PE spectra of Figs. 4(a)–4(d) represents a state-to-state transition from a specified J' rotational level of the intermediate VC* state to a specified J^+ rotational level of the $VC^+(X^3\Delta; v^+ = 0)$ ion ground state. The intense sharp peaks marked by asterisk in the figures are found to originate from UV-UV and/or UV-VIS two-photon ionization of V atoms because the intensities of these peaks were found to depend solely on the intensity of UV ω_2.

We have constructed the simulated spectra for the VIS-UV-PFI-PE spectra shown as the top blue spectra of Figs. 4(a)–4(d). The procedures used for the simulation of all VIS-UV-PFI-PE spectra measured in the present experiment are the same as those employed in previous studies. The J^+ assignments (marked on top of the simulated spectra) were based on the least square fits of the observed rotational photoionization transitions to a standard formula similar to Eq. (4). Similar to previous simulations, we

assume a Gaussian instrumental profile (FWHM = 1.2 cm^{-1}) for PFI-PE detection. The relative intensities of individual rotational peaks of the simulated spectrum were adjusted to follow those observed in the experimental PFI-PE spectra.

The simulated spectra show that the lowest J^+ values for all four spectra of Figs. 4(a)–4(d) are 1, indicating that the projected total electronic angular momentum along the inter-nuclear axis of VC^+ is $\Omega^+ = 1$. Thus, we conclude that the term symmetry for the $VC^+(X)$ ground state is $^3\Delta_1$. The least square fits of the observed rotational PFI-PE peaks to an standard transition formula similar to Eq. (4) also give the rotational constant $B_0^+ = 0.6330 \pm 0.0010$ cm^{-1} and the band origin $\nu_{00}^+ = 57512.3 \pm 0.8$ cm^{-1} for the $VC^+(X^3\Delta_1; v^+ = 0)$ ground state.

The $VC^+(^3\Delta)$ electronic state consists of three spin-orbit components with $\Omega^+ = 1$, 2 and 3.[50] In order to search for the spectrum for the excited $VC^+(^3\Delta_2)$ spin-orbit state, we have extended the VIS-UV-PFI-PE measurements to the total energy $\omega_1 + \omega_2$ range of 57,619.8–57,683.3 cm^{-1} by scanning UV ω_2 in the region of 35,915.0–35,973.5 cm^{-1}. The VIS-UV-PFI-PE spectra for $VC^+(^3\Delta_2; v^+ = 0; J^+)$ thus obtained via the selected $J' = 2.5$, $J' = 3.5$, $J' = 4.5$ and $J' = 5.5$ level of the intermediate VC* state are depicted as the lower black spectra in Figs. 5(a), 5(b), 5(c), and 5(d), respectively. In this and all the VIS-UV-PFI-PE measurements presented below, the VIS ω_1 excitation conditions were kept identical to that used for recording the spectra of Figs. 4(a)–4(d). That is, single rotational levels, $J' = 2.5$, $J' = 3.5$, $J' = 4.5$ and $J' = 5.5$, of the intermediate VC* state were selected by VIS ω_1 excitation at the Q(2.5), Q(3.5), Q(4.5), and Q(5.5) transitions, respectively. The background peaks marked by asterisks in Figs. 5(a)–5(d) were attributed to two-photon UV-VIS and/or UV-UV resonance enhanced photoionization of V atoms.

The simulated spectra (upper blue curves) with J^+-rotational assignments are shown in Figs. 5(a)–5(d) for comparison with the VIS-UV-PFI-PE spectra. The observation of the lowest $J^+ = 2$ value indicates that $\Omega^+ = 2$, confirming the VC^+ ions formed in this PFI-PE band is $VC^+(^3\Delta_2; v^+ = 0; J^+)$. The least square fits of the observed rotational PFI-PE peaks to a standard rovibonic transition formula yield the

rotational constant $B_0^+ = 0.6479 \pm 0.0042$ cm^{-1} and the band origin $\nu_{00}^+ = 57{,}656.2 \pm 0.8$ cm^{-1} for the $VC^+(X^3\Delta_2; v^+ = 0)$ excited spin-orbit state.

Figures 6(a), 6(b), 6(c), and 6(d) show the VIS-UV-PFI-PE spectra for the formation of $VC(X^3\Delta_3; v^+=0; J^+)$ (lower black curves) obtained via the respective J'=2.5, J'=3.5, J'=4.5 and J'=5.5 rotational levels of the intermediate VC* state and by scanning UV ω_2 in the range of 36,078.0-36,126.0 cm^{-1}. The upper blue curves of Figs. 6(a)–6(d) are the simulated spectra with J^+ -rotational assignments marked on top of the spectra. The J^+-rotational assignments based on the least square fits are useful for identifying the rotational PFI-PE transition peaks for the formation of $VC^+(^3\Delta_3; v^+ = 0; J^+)$ as well as the background peaks (marked by asterisks) originated from two-photon UV-VIS and/or UV-UV photoionization of V atoms. As shown in Figs. 6(a)–6(d), the lowest J^+ values are all found to be 3, indicating that $\Omega^+ = 3$. Thus, we conclude that the VIS-UV-PFI-PE spectra of Figs. 6(a)-6(d) are associated with the formation of the $VC^+(^3\Delta_3; v^+ = 0; J^+)$ spin-orbit state. The least square fits of the observed rotational PFI-PE transitions to a standard rovibrational transition formula have also provided the rotational constant $B_0^+ = 0.6330 \pm 0.0020$ cm^{-1} and the band origin $\nu_{00}^+ = 57813.2 \pm 0.8$ cm^{-1} for the $VC^+(^3\Delta_3; v^+ = 0)$ state.

The identification of the three spin-orbit components, $^3\Delta_1$, $^3\Delta_2$, and $^3\Delta_3$, in this experiment has firmly established the conclusion that the ground electronic state for $VC^+(X)$ is of $^3\Delta_1$ symmetry, which is consistent with the dominant ground state electronic configuration of $\ldots 8\sigma^2 3\pi^4 8\sigma^1 1\delta^1$. The electron occupancy of the 1δ orbital is less than half full; therefore, the spin-orbit component of the smaller Ω^+ value is predicted to be the lowest spin-orbit state according to the Hund's rule. This prediction is in agreement with the experimental observation.

3.4. VIS-UV-PFI-PE spectra for $VC^+(X^3\Delta_{1,2,3}; v^+ = 1)$

The VIS-UV-PIE spectrum for VC^+ of Fig. 3 reveals a second PIE step at the total energy range of $\omega_1 + \omega_2 = 58{,}374.7$-$58{,}417.4$ cm^{-1}. This observation was helpful in narrowing of the energy range for searching the VIS-UV-PFI-PE spectrum for $VC^+(X^3\Delta_{1,2,3}; v^+ = 1)$. Figures 7(a), 7(b), 7(c), and 7(d) show the

VIS-UV-PFI-PE spectra for VC($X^3\Delta_1$; $v^+ = 1$, J^+) (lower black curves) obtained via the respective J'=2.5, J'=3.5, J'=4.5 and J'=5.5 rotational levels of the intermediate VC* state and by scanning UV ω_2 in the energy range of 36,660.4-36,707.5 cm^{-1}.

The upper blue spectra of Figs. 7(a)–7(d) are the simulated spectra with the J^+-rotational assignment marked on top of the spectra. Two dominant peaks marked by asterisks were confirmed to arise from two-photon UV-VIS and/or UV-UV photoionization of V atoms. The simulated spectra show that the lowest J^+ value is 1, indicating that the ion state associated with the spectra of Fig. 7(a)–7(b) is the $VC^+(X^3\Delta_1; v^+=1)$ state. By fitting the observed rotational PFI-PE peaks to a standard formula similar to Eq. (4), we have determined the rotational constant $B_1^+ = 0.6272 \pm 0.0007$ cm^{-1} and the band origin $\nu_{10}^+ = 58397.5 \pm 0.8$ cm^{-1} for the $VC^+(X^3\Delta_1; v^+=1)$ ion state.

Since all three spin-orbit states $VC^+(X^3\Delta_{1,2,3}; v^+ = 0)$ were identified in the above PFI-PE measurements, we expect to observe the spectra for the VC^+ ($X^3\Delta_2$; $v^+=1$) and the VC^+ ($X^3\Delta_3$; $v^+=1$) states in addition to the VC^+ ($X^3\Delta_1$; $v^+ = 1$) state. Guided by the measured energy separations for the $VC^+(X^3\Delta_{1,2,3}; v^+ = 0)$ spin-orbit states, we have conducted a search for the VIS-UV-PFI-PE spectra for $VC^+(^3\Delta_2; v^+ = 1)$ and $VC^+(^3\Delta_3; v^+ = 1)$ at about 144 and 300 cm^{-1}, respectively, above the band origin of the PFI-PE band for the VC^+ ($^3\Delta_1$; $v^+ = 1$) state. Figures 8(a), 8(b), 8(c), and 8(d) depict the VIS-UV-PFI-PE spectra (lower black curves) for the formation of $VC^+(^3\Delta_2; v^+ = 1; J^+)$ obtained via the respective J'=2.5, J'=3.5, J'=4.5 and J'=5.5 rotational levels of the intermediate VC* state and by scanning UV ω_2 in the energy range of 36,802.6-36,856.0 cm^{-1}. The upper blue spectra shown in Figs. 8(a)–8(d) are the corresponding simulated spectra. The J^+ rotational assignments marked on top of the simulated spectra were obtained based on least square fits of the observed rotational transitions to a standard formula similar to Eq. (4). The peaks denoted by asterisks in the figures were confirmed to result from UV-VIS and/or UV-UV photoionizatiom of V atoms. All simulated spectra of Figs. 8(a)–8(d) show that the lowest J^+ value is 2, and thus the cationic state involved is the $VC^+(^3\Delta_2; v^+=1)$ state. The least square fits of the observed rotational peaks also yield the

rotational constant B_1^+ = 0.6323 ± 0.0012 cm^{-1} and the band origin ν_{10}^+ = 58,540.5 ± 0.8 cm^{-1} for the VC$^+$($^3\Delta_2$; v$^+$ = 1) ion state.

Figure 9(a), 9(b), 9(c), and 9(d) depict the VIS-UV-PFI-PE spectra for VC($^3\Delta_3$; v$^+$=1, J^+) obtained via the respective J'=2.5, J'=3.5, J'=4.5, and J'=5.5 rotational levels of the intermediate VC* state and by scanning UV ω_2 in the energy range of 36,962.0–37,007.4 cm^{-1}. The simulated spectra with J^+-rotational assignments are shown as the upper blue curves in the figures. One dominant peak denoted by asterisk was identified to arise from UV-VIS and UV-UV photoionization of V atoms. The simulated spectra show that the lowest J^+ level is 3, indicating that the associated cationic state is VC$^+$($^3\Delta_3$; v$^+$=1). The least square fits of the observed rotational PFI-PE peaks have allowed the determination of the rotational constant B_1^+ = 0.6270 ± 0.0012 cm^{-1} and the band origin ν_{10}^+ = 58,697.6 ± 0.8 cm^{-1} for the VC$^+$($^3\Delta_3$; v$^+$ = 1) ion state.

3.5. VIS-UV-PFI-PE spectra for VC$^+$ ($X^3\Delta_1$; v$^+$=2)

Guided by the vibrational spacing determined for the VC$^+$($X^3\Delta_1$; v$^+$ = 0) and VC$^+$($X^3\Delta_1$; v$^+$ = 1) states, we have research and successfully observed the VIS-UV-PFI-PE spectrum for the VC$^+$($X^3\Delta_1$; v$^+$ = 2) state in the total energy range of ω_1 + ω_2 = 59,249.4-59,298.6 cm^{-1}, which is about 873 cm^{-1} higher than the VIS-UV-PFI-PE band for VC$^+$($X\ ^3\Delta_1$; v$^+$ = 1) state. Figures 10(a), 10(b), 10(b), and 10(c) depict the VIS-UV-PFI-PE spectra for the formation of VC($X^3\Delta_1$; v$^+$=2; J^+) obtained via the respective J' = 2.5, J' = 3.5, and J' = 4.5 rotational levels of the intermediate VC* state and by scanning UV ω_2 in the energy range of 37,532.1-37,581.3 cm^{-1}. The simulated spectra with J^+-rotational assignments are shown as the upper blue curves. The peaks denoted by asterisk were identified as background structures arising from UV-VIS and/or UV-UV photoionization of V atoms. The simulated spectra show that the lowest J^+ value is 1, indicating that the cationic state formed is the VC$^+$($X^3\Delta_1$; v$^+$=2) state. The simulation also provide the rotational constant B_2^+ = 0.6264 ± 0.0023 cm^{-1} and the band origin ν_{20}^+ = 59,271.3 ± 0.8 cm^{-1} for the VC$^+$($^3\Delta_1$; v$^+$ = 2) state.

3.6. Analysis of energetic and spectroscopic constants

Considering that the adiabatic IE(VC) is defined as the energy between the neutral ground state VC($X^2\Delta_{3/2}$; $v^+ = 0$; $J'' = 3/2$) and the cationic ground state $VC^+(X^3\Delta_1$; $v^+ = 0$; $J^+=1$), we have determined the adiabatic IE(VC) = 57512.0 ± 0.8 cm^{-1} (7.13058 ± 0.00010 eV). To our knowledge, no experimental IE(VC) measurement has been made previously; and the previous IE(VC) value of 7.36 eV[13] available in the literature was obtained from theoretical density functional (DFT) calculations. The deviation of +0.23 eV observed between this DFT prediction and the present VIS-UV-PFI-PE measurement indicates that the DFT-based IE(VC) prediction is not accurate. The previous comparisons of experimental IE(MX) values determined by PFI-PE measurements with those obtained by DFT calculations show that the IE predictions by DFT calculations are not always reliable, the agreement for some cases was fortuitously good, but for some other cases was poor.

The IE of vanadium atom, IE(V) = 6.74633 ± 0.00012 eV, has been measured previously by Page *et al.*[28] On the basis of the thermochemical cycle, the accurate IE(VC) obtained here along with the known IE(V) allows the determination of the difference between 0 K bond dissociation energy of $VC^+(X^3\Delta_1)$ and that of VC($X^2\Delta_{3/2}$) to be $D_0(V^+–C) – D_0(V–C)$ = IE(V) – IE(VC) = –0.38425 ± 0.00012 eV. Gupta and Gingerich obtained a value of $D_0(V–C)$ = 4.34 ± 0.25 eV in a high-temperature Knudsen cell study.[51] Two values for $D_0(V^+–C)$ are found in the literature: $D_0(V^+–C)$ = 3.87 ± 0.14 eV[15] and 3.95 ± 0.04 eV[16], which were obtained in the guided ion beam mass spectrometric studies by Armentrout and co-workers. Combining these experimental values give two individual values (–0.47 ± 0.29 eV and –0.39 ± 0.25 eV) for $D_0(V^+–C)$ $–D_0(V–C)$; the latter value is in better agreement with the D_0 difference of -0.38425 ± 0.00012 eV obtained in the present PFI-PE measurements. The 8σ orbital in $VC(X^2\Delta)$ is a bonding orbital, the adiabatic ionization process would decrease its bond order (or strength) and the $VC^+(X^3\Delta)$ is expected to have a slightly longer and weaker bond, i.e., $D_0(V^+–C) – D_0(V–C)$ is a negative quantity.

The electronic energies associated with the three spin-orbit components $VC^+(X^3\Delta_1)$, $VC^+(X^3\Delta_2)$ and $VC^+(X^3\Delta_3)$, can be expressed as:

$$T_e = T_0 + A\Lambda\Sigma, \quad (5)$$

where T_e, T_0, Λ, Σ and A represents the term energy of spin-orbit state, electronic energy of the molecule without spin-orbit interaction, the projection of total orbital angular momentum along the inter-nuclear axis, the projection of total spin angular momentum along the inter-nuclear axis, and the spin-orbit coupling constant, respectively. $T_0 \approx T_{00} - \frac{1}{2}(\omega_e^+ - \omega_e")$, where T_{00} is the energy difference between VC($X\,^2\Delta$; v"=0) state and $VC^+(X\,^3\Delta; v^+=0)$ state, $\omega_e"$ (ω_e^+) is the harmonic vibrational frequency of ground state of VC (VC^+). According to Eq (5), the electronic energy for the $VC^+(X^3\Delta_1)$, $VC^+(^3\Delta_2)$ and $VC^+(^3\Delta_3)$ states are: $T_e(X^3\Delta_1) = T_0 - 2A$, $T_e(^3\Delta_2) = T_0$, and $T_e(^3\Delta_3) = T_0 + 2A$, respectively. Thus, the energy difference between $T_e(^3\Delta_3)$ and $T_e(X^3\Delta_1)$ is $4A$. The harmonic vibrational frequencies of spin-orbit components of VC($X\,^3\Delta$) state are expected with similar values. With the known $T_{00}(X^3\Delta_1; v^+=0)$ = 57,512.3 ± 0.8 $cm^{-1}$and $T_{00}(^3\Delta_3; v^+ = 0)$ = 57,813.2 ± 0.8 cm^{-1}, we have determined the spin-orbit coupling constant for $VC^+(X^3\Delta_{1,2,3})$ to be A = 75.2 ± 0.8 cm^{-1}. At the MRCI+Q/aug-cc-pVTZ (uncontracted basis functions) level, the SO coupling constant is predicted to be 79 cm^{-1}.

The vibrational energy of VC^+ cation can be expressed as:

$$G(v^+) = \omega_e^+\left(v^+ + \tfrac{1}{2}\right) - \omega_e^+ x_e^+\left(v^+ + \tfrac{1}{2}\right)^2. \quad (6)$$

The energy difference between adjacent vibrational states is written as:

$$\Delta G(v^+ + \tfrac{1}{2}) = G(v^+ + 1) - G(v^+) = \omega_e^+ - 2\omega_e^+ x_e^+ (v^+ + \tfrac{1}{2}) \quad (7)$$

For the $VC^+(X^3\Delta_1)$ spin-orbit state, the vibrational band origins, ν_{00}^+, ν_{10}^+ and ν_{20}^+ have been determined. These values have made possible the determination of the harmonic vibrational frequency ω_e^+ = 896.4 ± 0.8 cm^{-1} and anharmonicity constant $\omega_e^+x_e^+$ = 5.7 ± 0.8 cm^{-1} by least square fits of the band origins to Eq (6). The vibrational energy difference $\Delta G(1/2)$ = 885.1 ± 0.8 cm^{-1} and $\Delta G(3/2)$ = 873.8 ± 0.8 cm^{-1} can also be obtained by Eq. (7). For the $VC^+(^3\Delta_2)$ and the $VC^+(^3\Delta_3)$ spin-orbit electronic states, we report vibrational energy differences of $\Delta G(1/2)$ = 884.3 ± 0.8 cm^{-1} and $\Delta G(1/2)$ = 884.4 ± 0.8 cm^{-1}, respectively.

The rotational constant is dependent upon the v^+ vibrational level of VC^+ according to the formula:

$$B_v^+ = B_e^+ - \alpha_e^+(v^+ + \tfrac{1}{2}). \qquad (8)$$

With the measured B_0^+, B_1^+ and B_2^+ values for the $VC^+(X^3\Delta_1)$ ground state, we have obtained the equilibrium rotational constants B_e^+ = 0.6338 ± 0.0025 cm^{-1} and α_e^+ = 0.0033 ± 0.0007 cm^{-1} by least square fits of the rotational constants B_0^+, B_1^+, and B_2^+ according to Eq. (8). The B_e^+ constant thus obtained enables the determination of the equilibrium bond length r_e^+ = 1.6549 ± 0.0003 Å for the ionic $VC^+(X^3\Delta_1)$ ground electronic state. All energetic data and spectroscopic constants obtained in the present study are summarized in Table I.

In VIS-UV-PFI-PE measurements, such as the experiment on VC/VC^+ system presented here, the angular momentum (J') for the neutral rotational state can be selected and the angular momentum (J^+) for the ion rotational state can be determined. The rotational angular momentum change, $\Delta J^+ = J^+ - J'$, is of interest because it is a measure of the efficiency of energy conversion between the ejecting electron and the ion core. Based on the conservation of angular momentum, the observed ΔJ^+ change allows the determination of the orbital angular momentum for the ejected photoelectron. The intensity distribution of

the ΔJ^+ rotational PFI-PE transitions is a measure of the relative $J^+ \leftarrow J'$ photoionization cross sections. The intensity distributions of the ΔJ^+ rotational transitions observed here for the VC/VC^+ system are consistent with those found in the majority of the previous state-to-state PFI-PE studies, such as CH_3I/CH_3I^+, FeC/FeC^+, NiC/NiC^+, CoC/CoC^+, TiO/TiO^+, VN/VN^+, VCH/VCH^+ and NbC/NbC^+, showing that the rotational transition with the minimum $|\Delta J^+| = | J^+ - J' |$ value has the maximum intensity; and that the intensity of the rotational transition decrease as $|\Delta J^+|$ is increased. This observation can be rationalized by the channel coupling scheme, which has been shown to depend on the density of states or the rotational constant of the molecular system involved.[52] Previous PFI-PE experiments on diatomic molecules show that when the rotational constant was increased from 0.5 to 2 cm^{-1}, the maximum $|\Delta J^+|$ value was found to decrease from 10 to 6.[52] The maximum $|\Delta J^+|$ value observed in the VIS-UV-PFI-PE spectra obtained in the present study is about 5. This is consistent with the rotational constants of 0.63-0.66 cm^{-1} determined for the VC/VC^+ system.

3.7. Theoretical predictions for the r_e (r_e^+) and ω_e (ω_e^+) of VC/VC^+

The predicted equilibrium bond lengths r_e (r_e^+) and harmonic vibrational frequencies ω_e (ω_e^+) of VC($X^2\Delta$) (VC^+($X^3\Delta$)) calculated at the coupled cluster level, multi-reference configuration interaction, and B3LYP levels are summarized in Table II. The r_e values at CCSD(T)/aug-cc-pVXZ levels are in the range from 1.619 to 1.629 Å, and are reduced by about 0.02 Å when the core-valence correlation effect is included. The r_e values at the CCSDT (1.619 Å), CCSDTQ (1.626 Å) and MRCI+Q (1.611 Å) levels are very similar. The CCSD(T), CCSDT, and CCSDTQ's ω_e values range from 811 to 916 cm^{-1} and the MRCI+Q level predicts a slightly stronger VC bond, indicated by a larger ω_e of 925 cm^{-1} and a smaller r_e value. No experimental value for r_e and ω_e has been reported previously.

The r_e^+, ranging from 1.624 to 1.652 Å at the CCSD(T) level, comes fairly close to the experimental value of 1.6549 ± 0.0003 Å. The CCSDT and MRCI+Q values (r_e^+ = 1.653 and 1.654 Å) are almost the same as the experimental value, whereas the CCSDTQ prediction (1.666 Å) is too long. In the adiabatic

ionization process of VC ($X^2\Delta$), the electron in the bonding orbital (8σ) is removed. Thus, the $VC^+(X^3\Delta)$ cation is expected to have a weaker and longer bond. By comparing the harmonic vibrational frequency of VC ($X^2\Delta$) and $VC^+(X^3\Delta)$, it should give an insight into their relative bond strengths. The ω_e^+ values at the CCSD(T) and CCSDT level range from 926 to 1030 cm^{-1}, which deviate from the experimental value of 896.4 ± 0.8 cm^{-1} by ~30 to 140 cm^{-1} and are also larger than the ω_e values over 100 cm^{-1} (comparison is made at the same level of theory). Even at the CCSDT level, the ω_e^+ (926 cm^{-1}) is still larger than ω_e by 10 cm^{-1}, implying that the V^+–C bond is incorrectly predicted to be slightly stronger than the V–C bond. However, the ω_e^+ = 878 cm^{-1} at the CCSDTQ level is 18 cm^{-1} off from the experimental ω_e^+ (896.4 ± 0.8 cm^{-1}) and is also smaller than the ω_e value (911 cm^{-1}). As found in previous vibration frequency predictions for FeC/FeC^+ and CoC/CoC^+,[25,27] the inclusion of full triplet and quadruple excitations in the coupled-cluster theory are critical to give the correct harmonic force constant and hence vibrational frequencies of VC^+. The MRCI+Q ω_e^+ value of 886 cm^{-1} gets even closer to the experimental value and the deviation is just 10 cm^{-1}.

3.8. Theoretical predictions of IE(VC), D_0(V-C), D_0(V^+-C), ΔH°_{f0}(V^+-C), and ΔH°_{f298}(V^+-C)

It is of great interest to examine the performance of single-reference coupled cluster theory in energetic predictions for the VC/VC^+ system, which possesses of many low-lying excited states. The individual energy corrections ($\Delta E_{\text{extrapolated CBS}}$, ΔE_{CV}, ΔE_{ZPVE}, ΔE_{SO}, ΔE_{SR}, and ΔE_{HOC}) for the IE(VC), IE(V), D_0(V–C), and D_0(V^+–C) predictions using the CCSDTQ/CBS method are listed in Table III. The CCSDTQ/CBS prediction for IE(VC)=7.126 eV is found to be only 5 meV smaller than the measured IE(VC) = 7.13058 ± 0.00010 eV. The most significant contribution (ΔE_{HOC} = –44 meV) to IE(VC) is from the full triple and quadruple excitations beyond CCSD(T) wavefunction. On the other hand, the relativistic effect plays an important role to the CCSDTQ/CBS values for D_0(V–C) and D_0(V^+–C): it contributes negatively (ΔE_{SR} ~ –0.15 eV) to D_0(V–C) but positively (ΔE_{SR} ~ +0.14 eV) to D_0(V^+–C). The

CCSDTQ/CBS procedures also give an excellent prediction to the IE(V) value of 6.766 eV, which deviates from the experimental value[28] of 6.74633 ± 0.00012 eV by 20 meV.

Based on the CCSDTQ/CBS values of IE(VC) = 7.126 and IE(V) = 6.766 eV, we obtain a theoretical $D_0(V^+–C) – D_0(V–C)$ value of −0.360 eV. Both ΔE_{SR} and ΔE_{HOC} components (~0.29 and 0.063 eV) make huge contributions to the $D_0(V^+–C) – D_0(V–C)$ value, which is in excellent agreement with present PFI-PE experimental $D_0(V^+–C) – D_0(V–C)$ value of –0.38425 ± 0.00012 eV and that of –0.39 ± 0.25 eV obtained based on the previous guided ion beam measurements. However, the good agreement between CCSDTQ/CBS value (–0.360 eV) and the latter value (–0.39 ± 0.25 eV) is most likely fortuitous as the individual $D_0(V^+–C)$ and $D_0(V–C)$ experimental values do not yield a reliable set of $\Delta H^\circ_f(VC)$ and $\Delta H^\circ_f(VC^+)$ values when compared with the CCSDTQ predictions (see discussion below).

The respective ΔH^o_{f0} values for $VC(^2\Delta)$ and $VC^+(^3\Delta)$ can be derived using the experimentally determined $D_0(V–C)$[51] and $D_0(V^+–C)$[15,16] values and the known values of $\Delta H^o_{f0}(V)$, $\Delta H^o_{f0}(V^+)$, and $\Delta H^o_{f0}(C)$.[48] Based on the $D_0(V–C)$ = 4.34 ± 0.25 eV (419 ± 24 kJ mol^{-1})[51] and the known values for $\Delta H^o_{f0}(V)$= 512.2 kJ mol^{-1} and $\Delta H^o_{f0}(C)$=711.2,[48] an experimental value for $\Delta H^o_{f0}(VC)$ = 804 ± 24 kJ mol^{-1} (the value is rounded up to no decimal place) is obtained. Combining this $\Delta H^o_{f0}(VC)$ value with the present IE(VC) = 7.13058 ± 0.00010 eV and the 298 K thermal corrections from the CCSDTQ vibrational frequencies of VC/VC$^+$, we obtain a set of experimental values for $\Delta H^o_{f0}(VC)$ = 804 ± 24, $\Delta H^o_{f298}(VC)$ = 809 ± 24, $\Delta H^o_{f0}(VC^+)$ = 1492 ± 24, and $\Delta H^o_{f298}(VC^+)$ = 1497 ± 24 kJ mol^{-1} (Table IV). Compared with the CCSDTQ predictions of $\Delta H^o_{f0}(VC)$ = 835.2, $\Delta H^o_{f298}(VC)$ = 840.4, $\Delta H^o_{f0}(VC^+)$ = 1522.8, and $\Delta H^o_{f298}(VC^+)$ = 1528.0 kJ mol^{-1}, the experimental ΔH^o_f values are consistently smaller than the CCSDTQ/CBS values by over 30 kJ mol^{-1}. This suggests that the $D_0(V–C)$ value of 4.34 ± 0.25 eV by Gupta and Gingerich[51] is likely too high. Similarly, based on the $D_0(V^+–C)$ values[15] of 3.87 ± 0.14 eV and the known values for $\Delta H^o_{f0}(V^+)$ = 1163.1 kJ mol^{-1} (by adding experimental $\Delta H^o_{f0}(V)$ and IE(V) values together) and $\Delta H^o_{f0}(C)$ = 711.2, an experimental value for $\Delta H^o_{f0}(VC^+)$ = 1500.9 ± 14 kJ mol^{-1} are obtained. This $\Delta H^o_{f0}(VC^+)$ value is still

smaller than the CCSDTQ/CBS value by over 20 kJ mol^{-1}. If the $D_0(V^+–C)$ values[16] of 3.95 ± 0.04 eV is used, another set of experimental values for $\Delta H^o_{f0}(VC)$ = 805.2 ± 4, $\Delta H^o_{f298}(VC)$ = 810.4 ± 4, $\Delta H^o_{f0}(VC^+)$ = 1493.2 ± 4, and $\Delta H^o_{f298}(VC^+)$ = 1498.4 ± 4 kJ mol^{-1} are found (Table IV). This set of ΔH^o_f values is also smaller than the CCSDTQ/CBS predictions by ~30 kJ mol^{-1}. Compared with the CCSDTQ/CBS value of $D_0(V^+–C)$=3.663 eV, the experimental $D_0(V^+–C)$ values[15,16] of 3.87 ± 0.14 and 3.95 ± 0.04 eV are likely too high, it is logical to see that the $\Delta H^o_{f0}(VC^+)$ values deduced from these experimental $D_0(V^+–C)$ values are lower, given that the experimental values for ΔH^o_{f0} (V^+) and ΔH^o_{f0} (C) are known precisely.

In view of the excellent agreement between the CCSDTQ/CBS predictions and current experimental IE(VC) value, the CCSDTQ/CBS values for $D_0(V–C)$ = 4.023 eV, $D_0(V^+–C)$=3.663 eV and $D_0(V^+–C) – D_0(V–C)$ = −0.360 eV should form a consistent and reliable set of thermochemical data for the VC/VC^+ system. Although the CCSDTQ/CBS value for $D_0(V^+–C) – D_0(V–C)$ value is in agreement with the experimentally derived value of −0.39 ± 0.25 eV, the ΔH^o_f values derived from these experimental $D_0(V–C)$ and $D_0(V^+–C)$ values[15,16,51] are not consistent with the CCSDTQ predictions.

5. Conclusions

We have performed two-color VIS-UV laser PIE and PFI-PE study on cold VC molecules prepared by a supersonically cooled laser ablation source. The rotationally selected and resolved state-to-state PFI-PE spectra for VC^+ allow unambiguous spectroscopic analyses and rotational assignments, confirming that the ionic $VC^+(X)$ ground state is of $^3\Delta_1$ symmetry. The analysis of VIS-UV-PFI-PE spectra for the $VC^+(X^3\Delta_1; v^+ = 0\text{-}2; J^+)$, $VC^+(X^3\Delta_2; v^+ = 0\text{-}1; J^+)$ and $VC^+(X^3\Delta_2; v^+ = 0\text{-}1; J^+)$ states has enabled the determination of highly precise values for the IE(VC), the difference in 0 K bond dissociation energy between the $VC^+(X^3\Delta_1)$ cation and the $VC(X^2\Delta_{3/2})$ neutral, the SO coupling constant, and the vibrational and rotational constants. These energetic and spectroscopic data have been used to benchmark predictions calculated based on the CCSDTQ/CBS procedures. The CCSDTQ/CBS prediction of IE(VC) = 7.126 eV is in excellent agreement

with the value of 7.13058 ± 0.00010 eV measured from the rotationally resolved state-to-state PFI-PE spectra. The CCSDTQ values for r_e^+ = 1.666 Å and ω_e^+=878 cm^{-1} are also in good accord with the experimental r_e^+ = 1.6549 ± 0.0003 Å and ω_e^+ = 896.4 ± 0.8 cm^{-1}. The comparison between the CCSDTQ and experimental ω_e^+ suggests that the inclusion of full triplet and quadruple excitations in the coupled-cluster method are critical to obtain the reliable harmonic force constant for $VC^+(^3\Delta)$. Based on the available D_0(V–C) and $D_0(V^+–C)$ values,[15,16,51] we obtained experimental ΔH^o_f values for VC and VC^+, which are found to deviate from the CCSDTQ/CBS values by 20 – 30 kJ mol^{-1}. Given the excellent agreement between the CCSDTQ/CBS predictions and current experimental IE(VC) value, we recommend CCSDTQ/CBS values of D_0(V–C) = 4.023 and $D_0(V^+–C)$ = 3.663 eV, and also the ΔH^o_{f0}(VC) = 835.2, ΔH^o_{f298}(VC) = 840.4, $\Delta H^o_{f0}(VC^+)$ = 1522.8, and $\Delta H^o_{f298}(VC^+)$ = 1528.0 kJ mol^{-1} to be reliable sets of thermochemical data.

Acknowledgements:

This work was supported by the NSF Grant No. CHE 0910488.

References:

1. B. Simard, P. A. Hackett and W. J. Balfour, *Chem. Phys. Lett.*, 1994, **230**, 103.
2. M. R. Sievers, Y. M. Chen and P. B. Armentrout, *J. Chem. Phys.*, 1996, **105,** 6322.
3. B. Simard, P. I. Presunka, H. P. Loock, A. Bérces and O. Launila, *J. Chem. Phys*., 1997, **107**, 307.
4. O. Krechkivska and M. D. Morse, *J. Phys. Chem. A*., 2013, **117**, 13284.
5. S. T. Oyama, *Chemistry of transition metal carbides and nitrides*. (springer, 1996).
6. J. F. Harrison, *Chem. Rev.*, 2000, **100**, 679.
7. R. J. Van Zee, J. J. Bianchini and W. Jr. Weltner, *Chem. Phys. Lett.*, 1986, **127**, 314.
8. Y. M. Hamrick and W. Jr. Weltner., *J. Chem. Phys.*, 1991, **127**, 3371.

9. S. M. Matter, *J. Phys. Chem*., 1993, **97**, 3171.

10. R. G. A. R. Maclagan and G. E. Scuseria, *Chem. Phys. Lett*., 1996, **262**, 87.

11. D. Majumdar and K. A. Balasubramaian, *Mol. Phys*., 2013, **101**, 1369.

12. A. Kalemos, T. H. Dunning Jr. and A. Mavridis, *J. Chem. Phys*., 2005, **123**, 014301.

13. G. L. Gutsev, L. Andrews and C. W. Bauschlicher Jr., *Theor. Chem. Acc*., 2003, **109**, 298.

14. I. S. K. Kerkines and A. Mavridis, *Mol. Phys.*, 2004, **102**, 2451.

15. D. E. Clemmer, J. L. Elkind, N. Aristov and P. B. Armentrout, *J. Chem. Phys.*, 1991, **95**, 3387.

16. N. Aristove and P. B. Armentrout, *J. Am. Chem. Soc*., 1986, 108, 1806.

17. Z. H. Luo, Z. Zhang, H. Huang, Y.- C. Chang and C. Y. Ng, *J. Chem. Phys.*, 2014, **140**, 181101.

18. Y.-C. Chang, C.-S. Lam, B. Reed, K.-C. Lau, H. T. Liou and C. Y. Ng, *J. Phys. Chem. A*, 2009, **113**, 4242.

19. Y.-C. Chang, X. Shi, K.-C. Lau, Q.-Z. Yin, H. T. Liou and C. Y. Ng, *J. Chem. Phys.*, 2010, **133**, 054310.

20. H. Huang, Y.-C. Chang, Z. H. Luo, X. Shi, C.-S. Lam, K.-C. Lau and C. Y. Ng, *J. Chem. Phys.*, 2013, **138**, 094301.

21. H. Huang, Z. H. Luo, Y.-C. Chang, K.-C. Lau and C. Y. Ng, *J. Chem. Phys*., 2013, **138**, 174309.

22. H. Huang, Z. H. Luo, Y.-C. Chang, K.-C. Lau and C. Y. Ng, *Chin. J. Chem. Phys.*, 2013, **26**, 669.

23. Z. H. Luo, H. Huang, Z. Zhang, Y.-C. Chang and C. Y. Ng, *J. Chem. Phys.*, 2014, **141**, 024304.

24. Z. H. Luo, H. Huang, Y.-C. Chang, Z. Zhang, Q.-Z. Yin and C. Y. Ng, *J. Chem. Phys.*, 2014, **141**, 144307.

25. K.-C. Lau, Y.-C. Chang, C.-S. Lam and C. Y. Ng, *J. Phys. Chem. A*, 2009, **113**, 14321.

26. K.-C. Lau, Y.-C. Chang, X. Shi and C. Y. Ng, *J. Chem. Phys.*, 2010, **133**, 114304.

27. K.-C. Lau, Y. Pan, C.-S. Lam, H. Huang, Y.-C. Chang, Z. H. Luo, X. Y. Shi and C. Y. Ng, *J. Chem. Phys.*, 2013, **138**, 094302.

28. R. H. Page and S. Gudenman, *J. Opt. Soc. Am. B*, 1990, **7**, 1761.

29. T. G. Dietz, M. A. Duncan, D. E. Powers and R. E. smalley, *J. Chem. Phys.*, 1981, **74**, 6511.

30. Y. C. Chang, H. Xu, Y.-T. Xu, Z. Lu, Y.-H. Chiu, D. J. Levandier and C. Y. Ng, *J. Chem. Phys.*, 2011, **134**, 201105.

31. Y. C. Chang, Y. Xu, Z. Lu, H. Xu and C. Y. Ng, *J. Chem. Phys.*, 2012, **137**, 104202.

32. J. D. Watts, J. Gauss and R. J. Bartlett, *J. Chem. Phys.*, 1993, **98**, 8718.

33. M. Rittby and R. J. Bartlett, *J. Phys. Chem.*, 1988, **92**, 3033.

34. K. A. Peterson and T. H. Dunning, Jr., *J. Chem. Phys.*, 2002, **117**, 10548.

35. N. B. Balabanov and K. A. Peterson, *J. Chem. Phys.*, 2005, **123**, 064107.

36. K. A. Peterson, D. E. Woon and T. H. Dunning, Jr., *J. Chem. Phys.*, 1994, **100**, 7410.

37. T. Helgaker, W. Klopper, H. Koch and J. Noga, *J. Chem. Phys.*, 1997, **106**, 9639.

38. A. Halkier, T. Helgaker, P. Jorgensen, W. Klopper, H. Koch, J. Olsen and A. K. Wilson, *Chem. Phys. Lett.*, 1998, **286**, 243.

39. K.-C. Lau and C. Y. Ng, *J. Chem. Phys.*, 2005, **122**, 224310; 2006, **124**, 044323; *Chin. J. Chem. Phys.*, 2006, **19**, 29; *Acc. Chem. Res.*, 2006, **39**, 823; *J. Chem. Phys.*, 2011, **135**, 246101.

40. M. Douglas and N. M. Kroll, *Ann. Phys.*, 1974, **82**, 89.

41. G. Jansen and B. A. Hess, *Phys. Rev. A*, 1989, **39**, 6016.

42. W. A. de Jong, R. J. Harrison and D. A. Dixon, *J. Chem. Phys.*, 2001, **114**, 48.

43. A. Berning, M. Schweizer, H.-J. Werner, P. J. Knowles and P. Palmieri, *Mol. Phys.*, 2000, **98**, 1823.

44. C. E. Moore, "Atomic energy levels," Natl. Bur. Stand. (U.S.) Circular No. 467 (U.S. Government Printing Office, Washington, DC, 1949).

45. H.-J. Werner, P. J. Knowles, R. Lindh, F. R. Manby, M. Schütz *et al.*, MOLPRO, version 2010.1, a package of *ab initio* programs, 2010, see http://www.molpro.net.

46. M. Kállay, MRCC, a string-based quantum chemical program suite, 2001. See also M. Kállay and P. R.

Surján, *J. Chem. Phys*., 2001, **115**, 2945 as well as www.mrcc.hu.

47. L. A. Curtiss, K. P. Raghavachari, C. Redfern and J. A. Pople, *J. Chem. Phys.*, 1997, **106**, 1063.

48. M. W. Chase, Jr., *J. Phys. Chem. Ref. Data Monogr. 9*, 1998; S. G. Lias, J. E. Bartmess, J. F. Liebman, J. L. Holmes, R. D. Levin, and W. G. Mallard, *J. Phys. Chem. Ref. Data 17*(*Suppl. 1*), 1988.

49. NIST Atomic Spectra Database, http://physcis.nist.gov/cgi-bin/ASD/line

50. W. H. Hocking, M. C. L. Gerry and A. J. Merer, *Can. J. Phys*., 1979, **57**, 54.

51. S. K. Gupta and K. A. Gingerish. *J. Chem. Phys*., 1981, **74**, 3584.

52. E. W. Schlag, *ZEKE Spectroscopy*. (Cambridge University Press, Cambridge, 1996).

Figure Captions:

Figure 1 The excitation spectrum (lower spectrum) for the [21.72] $\Omega' = 2.5 \leftarrow X\ ^2\Delta_{3/2}$ transition band. The spectrum was recorded by means of two-color VIS-UV phtoionization scheme, in which UV ω_2 was set at 47,169.8 cm^{-1} and VIS ω_1 was scanned in the energy range of 21,693-21,724 cm^{-1}. The simulated spectrum (upper spectrum) was constructed assuminga Gaussian instrumental profile (FWHM = 0.4 cm^{-1}) for optical excitation and a Boltzmann rotational distribution (rotational temperature = 30 K) of a VC ($X^2\Delta_{3/2}$) molecular beam. The rotational assignment is marked on the top of simulated spectrum. The rotation transitions Q(2.5), Q(3.5), Q(4.5), and Q(5.5) (marked by downward pointing arrows) are selected for rotationally selected VIS-UV-PIE and VIS-UV-PFI-PE measurements.

Figure 2 Upper spectrum: TOF mass spectrum obtained by setting VIS ω_1 = 21717.27 cm^{-1} and UV ω_2 = 47169.8 cm^{-1}.The $^{51}V^+$, $^{51}V^{12}C^+$, and $^{51}V^{16}O^+$ cations, are observed. Lower spectrum: TOF mass spectrum observed under the same experimental conditions for recording the upper spectrum except the VIS ω_1 was blocked. The comparison of the upper and lower spectra shows thar $^{51}V^{12}C^+$ ions are only product by VIS-UV photoionization.

Figure 3 The photoionization efficiency (PIE) spectrum for $VC^+(X^3\Delta; v^+ = 0$ and 1) recorded by means of two-color VIS-UV photoionization, in which VIS ω_1 was set at 21,717.27 cm^{-1}, while UV ω_2 was scanned in the range of 35643.16-37,000.0 cm^{-1}. The bottom energy scale represents the UV (ω_2) energy, while the top energy scale represents the total ($\omega_1 + \omega_2$) energy.

Figure 4 VIS-UV-PFI-PE spectra for the $VC^+(X^3\Delta_1; v^+ = 0; J^+)$ cationic states in the total ($\omega_1 + \omega_2$) energy range of 57,485 – 57,544 cm^{-1} (top energy scale) obtained via the (a) J'=2.5, (b) J'=3.5, (c) J'=4.5, and (d) J'=5.5 rotational levels of the intermediate VC* state. The corresponding UV ω_2 were scanned in the range of 35,744.5 – 35,834.2 cm^{-1} (bottom energy scale). The J' levels were selected by setting VIS ω_1 at the Q(2.5), Q(3.5), Q(4.5) and Q(5.5) transitions as shown in

Fig. 1. The simulated spectra shown as upper blue spectra in (a)-(c) were constructed by assuming a Gaussian instrumental line profile with FWHM = 1.2 cm^{-1} for PFI-PE detection.

Figure 5 VIS-UV-PFI-PE spectra and simulated spectra for the $VC^+(X^3\Delta_2; v^+ = 0; J^+)$ cationic states in the total ($\omega_1 + \omega_2$) energy range of 57,619.8-57,683.3 cm^{-1} (top energy scale) obtained via the (a) J' = 2.5, (b) J' = 3.5, (c) J' = 4.5, and (d) J' = 5.5 rotational levels of the intermediate VC* state. The corresponding UV ω_2 scanning range is 35,915.0 – 35,973.5 cm^{-1} (bottom energy scale). The J' levels were selected by setting VIS ω_1 at the Q(2.5), Q(3.5), Q(4.5) and Q(5.5) transitions shown in Fig. 1.

Figure 6 VIS-UV-PFI-PE spectra and simulated spectra for the $VC^+(X^3\Delta_3, v^+=0, J^+)$ cationic states in the total ($\omega_1 + \omega_2$) energy range of 57,787.8-57,835.8 cm^{-1} (top energy scale) obtained via the (a) J'=2.5, (b) J'=3.5, (c) J'=4.5 and (d) J'=5.5 rotational level of the intermediate VC* state. The corresponding UV ω_2 scanning range is 36078.0 – 36126.0 cm^{-1} (bottom energy scale). The J' levels were selected by setting VIS ω_1 at the Q(2.5), Q(3.5), Q(4.5) and Q(5.5) transitions shown in Fig. 1.

Figure 7 VIS-UV-PFI-PE spectra and simulated spectra for the $VC^+(X^3\Delta_1; v^+ = 1; J^+)$ cationic states in the total ($\omega_1 + \omega_2$) energy range of 58,370.2-58,417.3 cm^{-1} (top energy scale) obtained via the (a) J'=2.5, (b) J'=3.5, (c) J'=4.5 and (d) J'=5.5 rotational levels of the intermediate VC* state. The corresponding UV ω_2 scanning range is 36,660.4 – 36,707.5 cm^{-1} (bottom energy scale). The J' levels were selected by setting VIS ω_1 at the Q(2.5), Q(3.5), Q(4.5) and Q(5.5) transitions shown in Fig. 1.

Figure 8 Rovibronically resolved VIS-UV-PFI-PE spectra and simulated spectra for the $VC^+(X^3\Delta_2, v^+=1, J^+)$ cationic states in the total ($\omega_1 + \omega_2$) energy range of 58512.4-58565.8 cm^{-1} (top energy scale) obtained via the (a) J'=2.5, (b) J'=3.5, (c) J'=4.5 and (d) J'=5.5 rotational levels of the intermediate VC* state. The corresponding UV ω_2 scanning range is 36,802.6 – 36,856.0 cm^{-1}.

The J' levels were selected by setting VIS ω_1 at the Q(2.5), Q(3.5), Q(4.5) and Q(5.5) transitions shown in Fig. 1.

Figure 9 VIS-UV-PFI-PE spectra and simulated spectra for the $VC^+(X^3\Delta_3, v^+=1, J^+)$ cationic states, in the total (ω_1+ ω_2) energy range of 58,671.8-58,725.0 cm^{-1} (top energy scale) obtained via the (a) J'=2.5, (b) J'=3.5, (c) J'=4.5 and (d) J'=5.5 rotational levels of the intermediate VC* state. The corresponding UV ω_2 scanning range is36,962.0 – 37,004.4 cm^{-1}. The J' levels were selected by setting VIS ω_1 at the Q(2.5), Q(3.5), Q(4.5), and Q(5.5) transitions shown in Fig. 1.

Figure 10 Rovibronically resolved VIS-UV-PFI-PE spectra and simulated spectra for the $VC^+(X^3\Delta_1, v^+=2, J^+)$ cationic states in the total (ω_1+ ω_2) energy range of 59,243.5-59,292.7 cm^{-1} (top energy scale) obtained via the (a) J'=2.5, (b) J'=3.5, and (c) J'=4.5 of rotational levels of the intermediate VC* state. The corresponding UV ω_2 scanning range is 37,532.1 – 37,581.3 cm^{-1}. The J' levels were selected by setting VIS ω_1 at the Q(2.5), Q(3.5), and Q(4.5) transitions shown in Fig. 1.

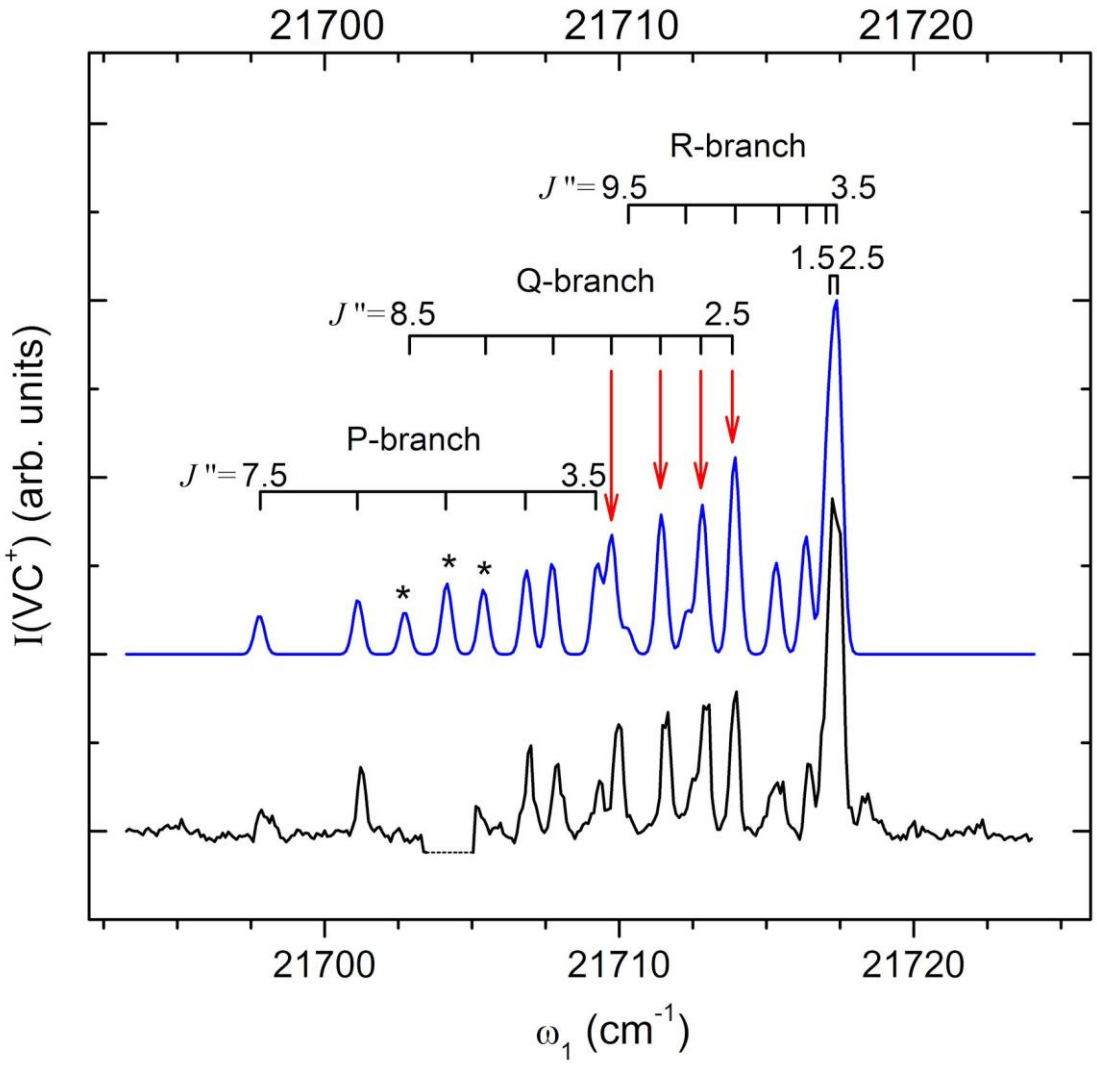

Figure 1

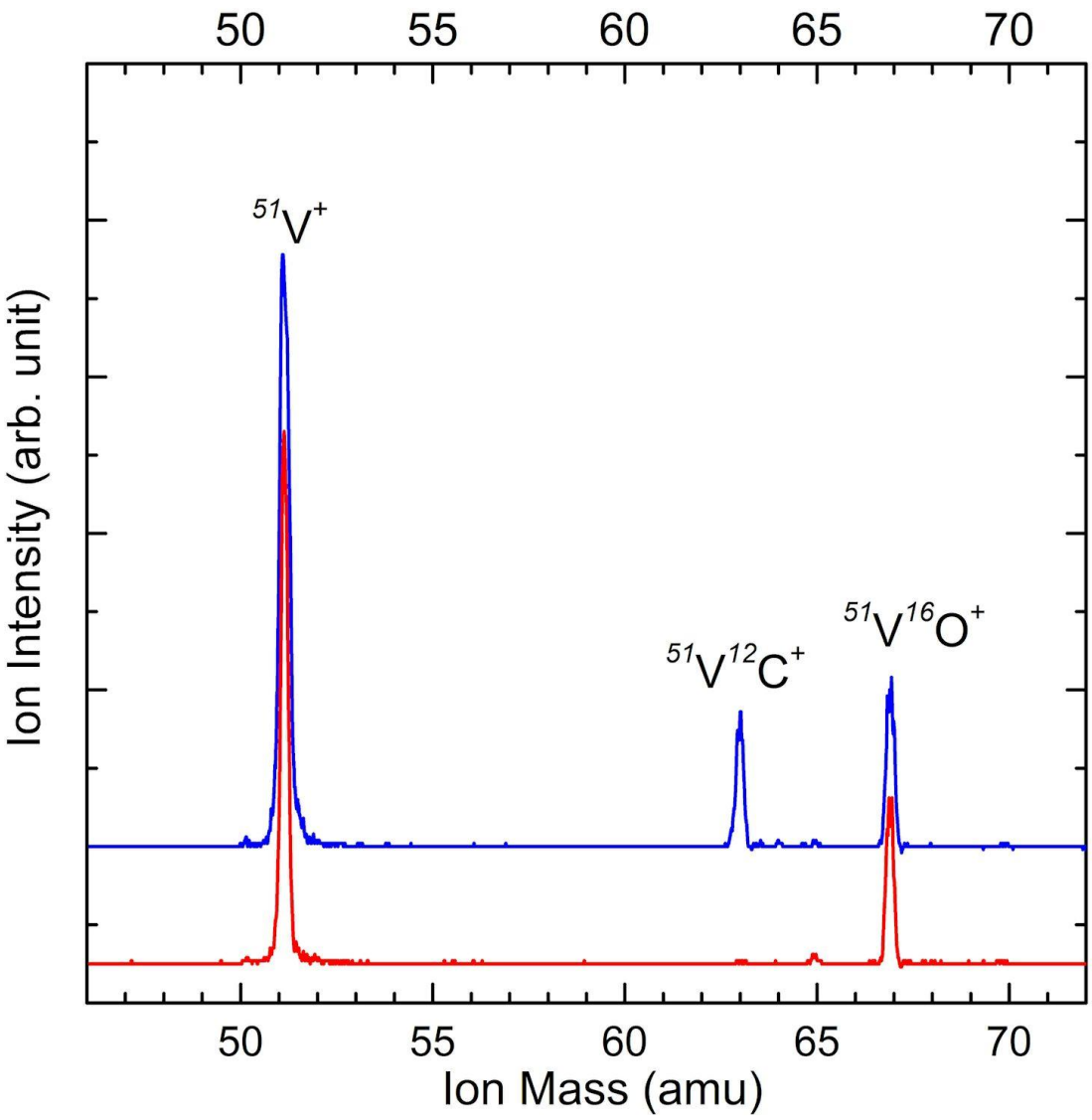

Figure 2

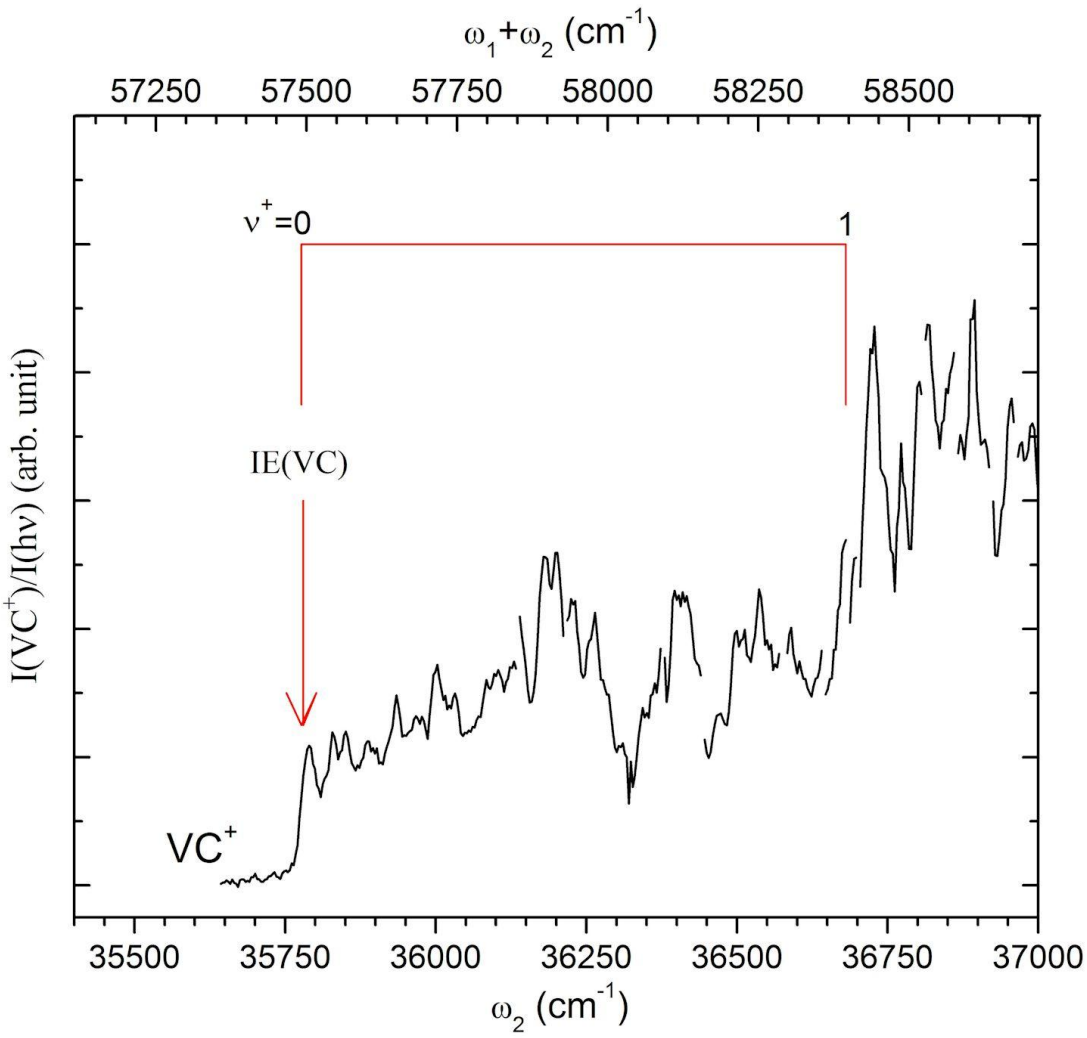

Figure 3

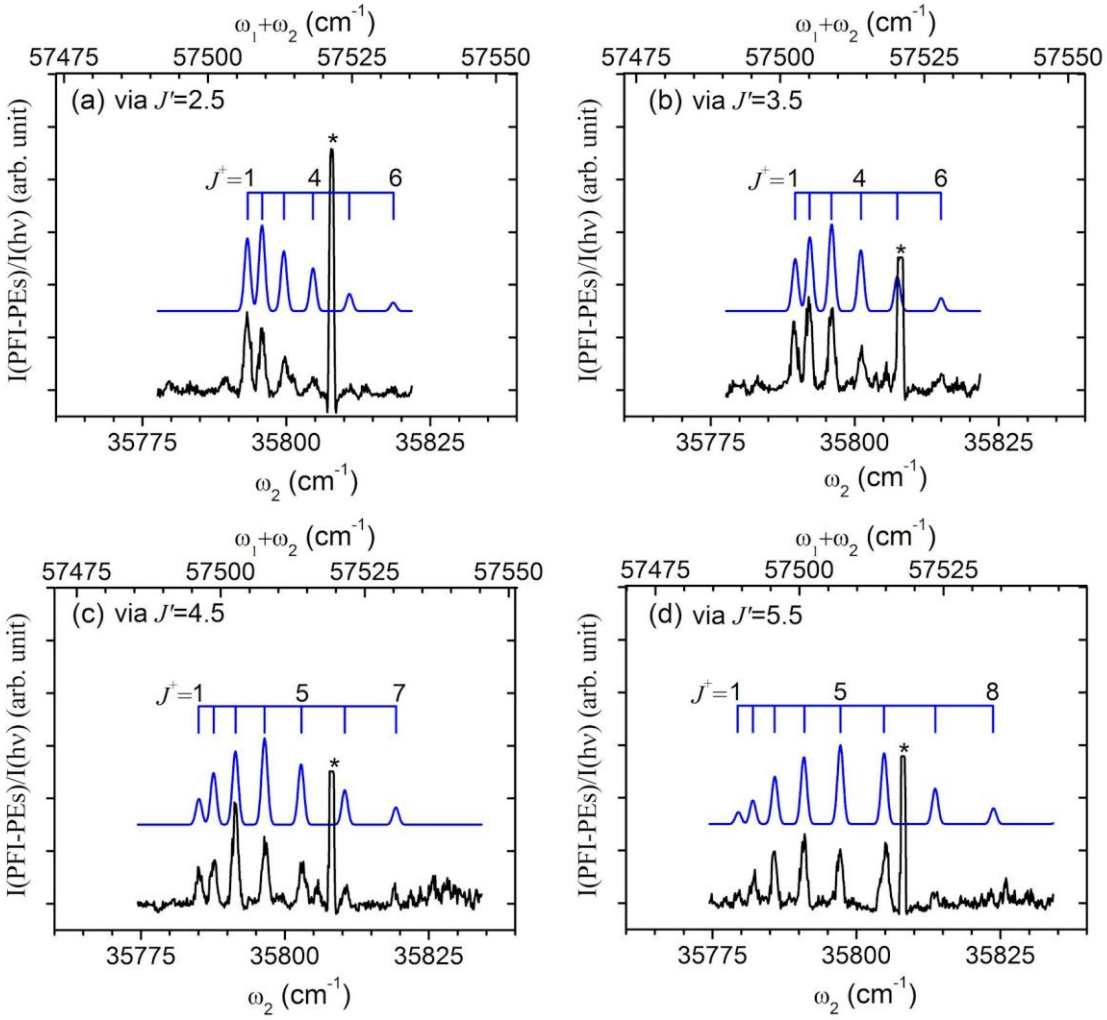

Figure 4

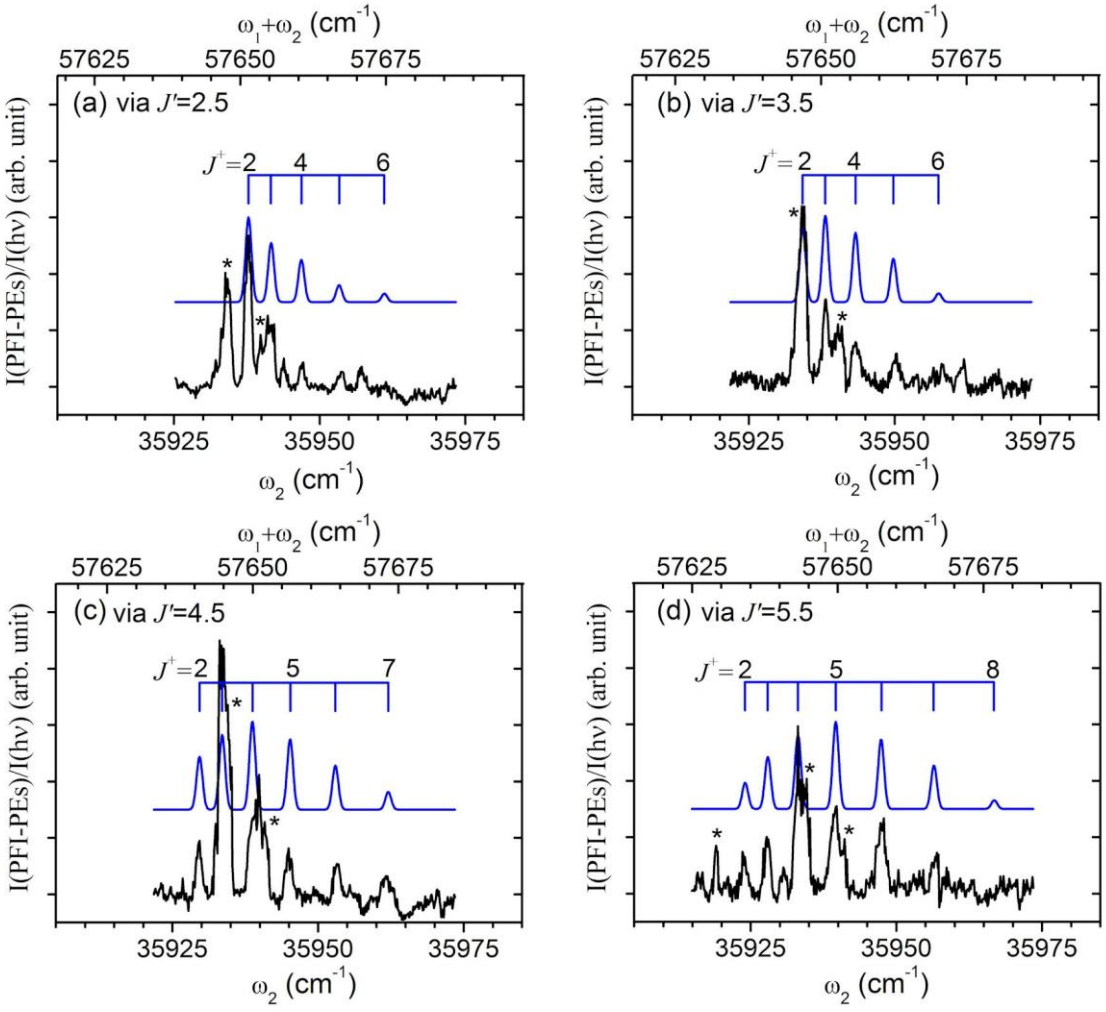

Figure 5

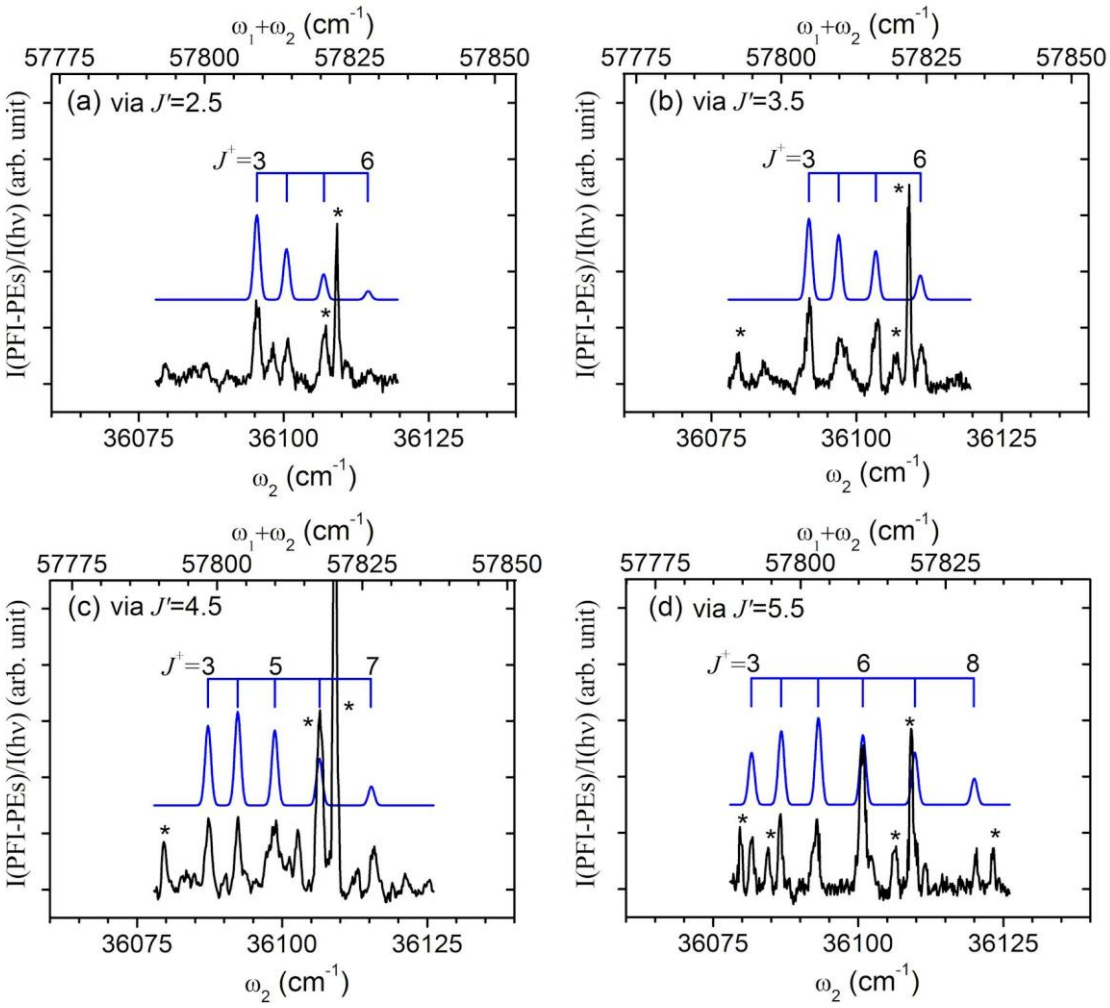

Figure 6

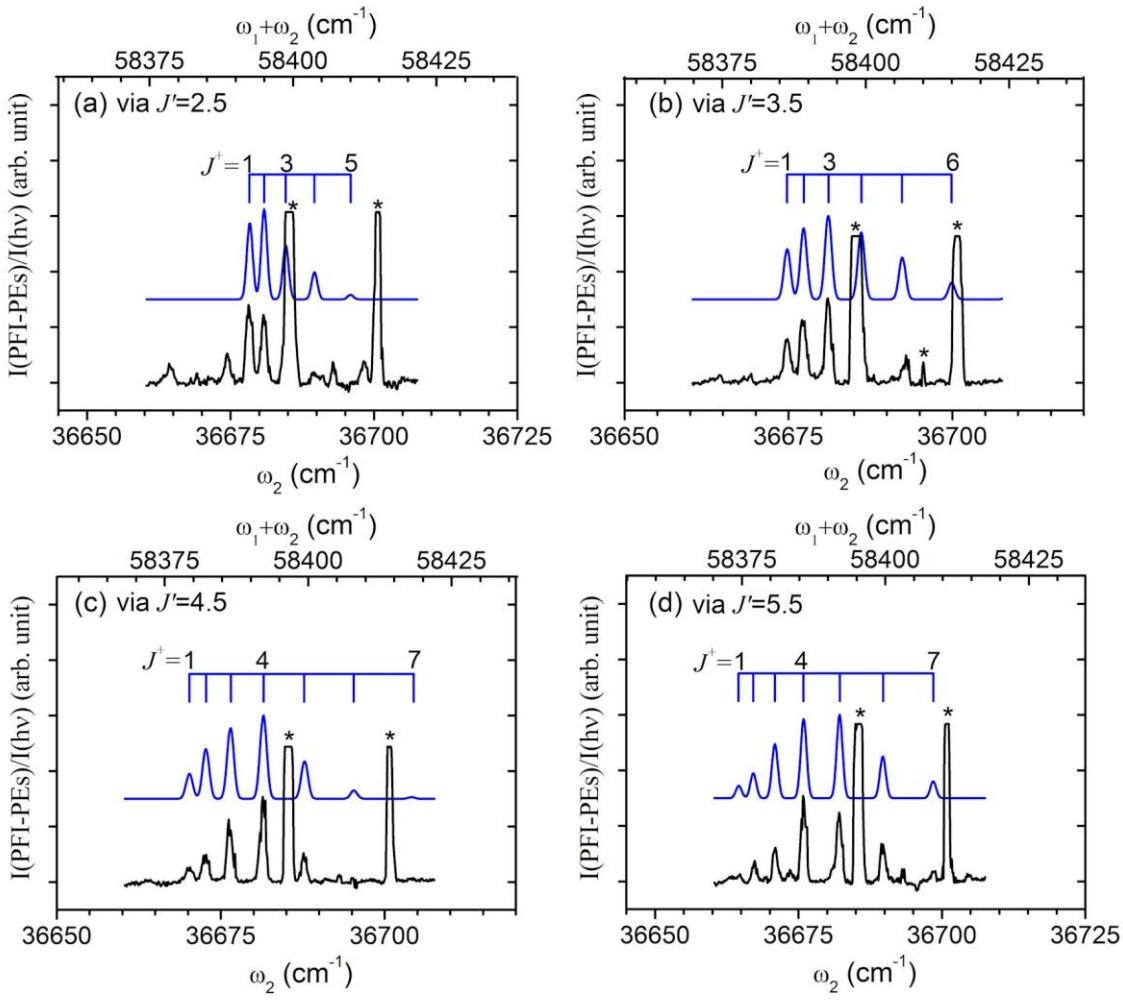

Figure 7

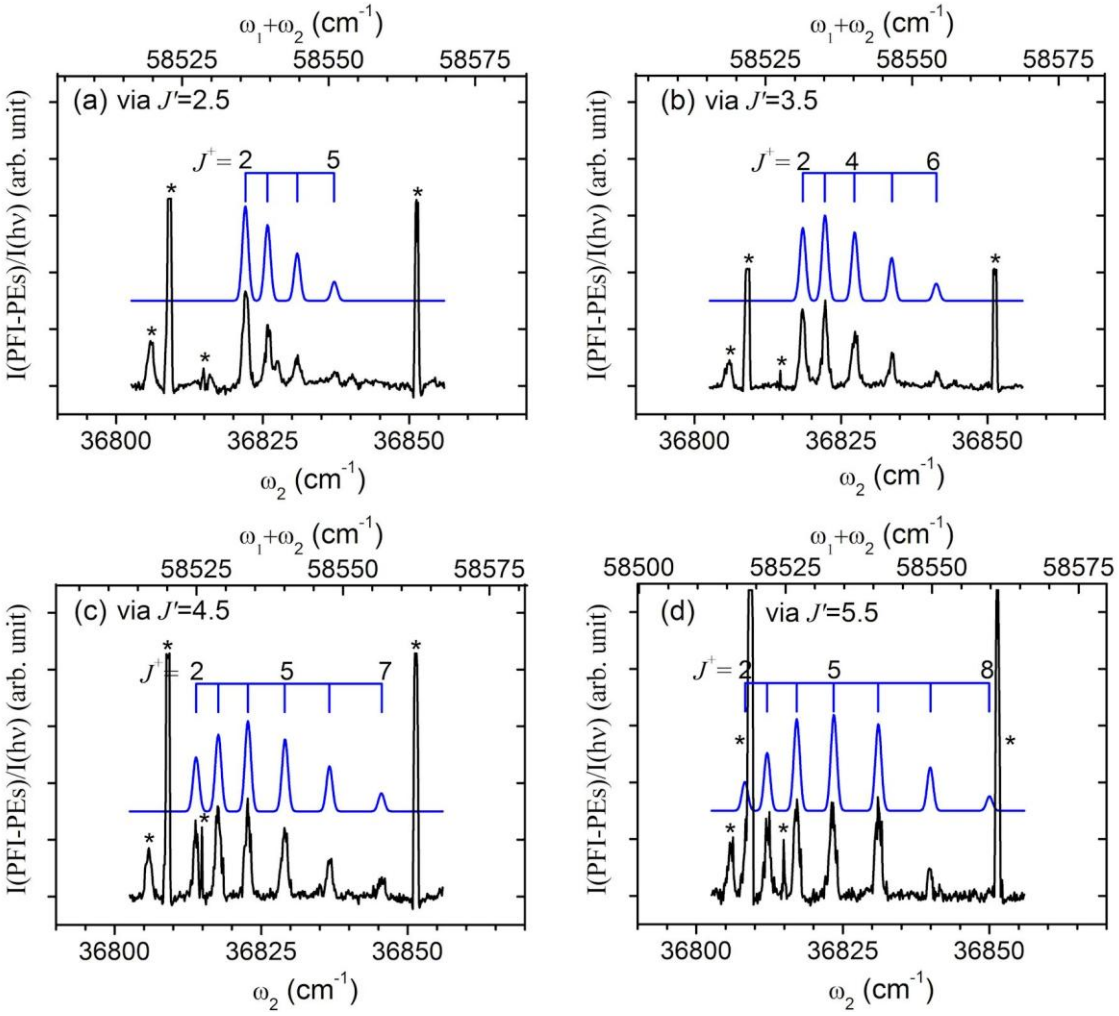

Figure 8

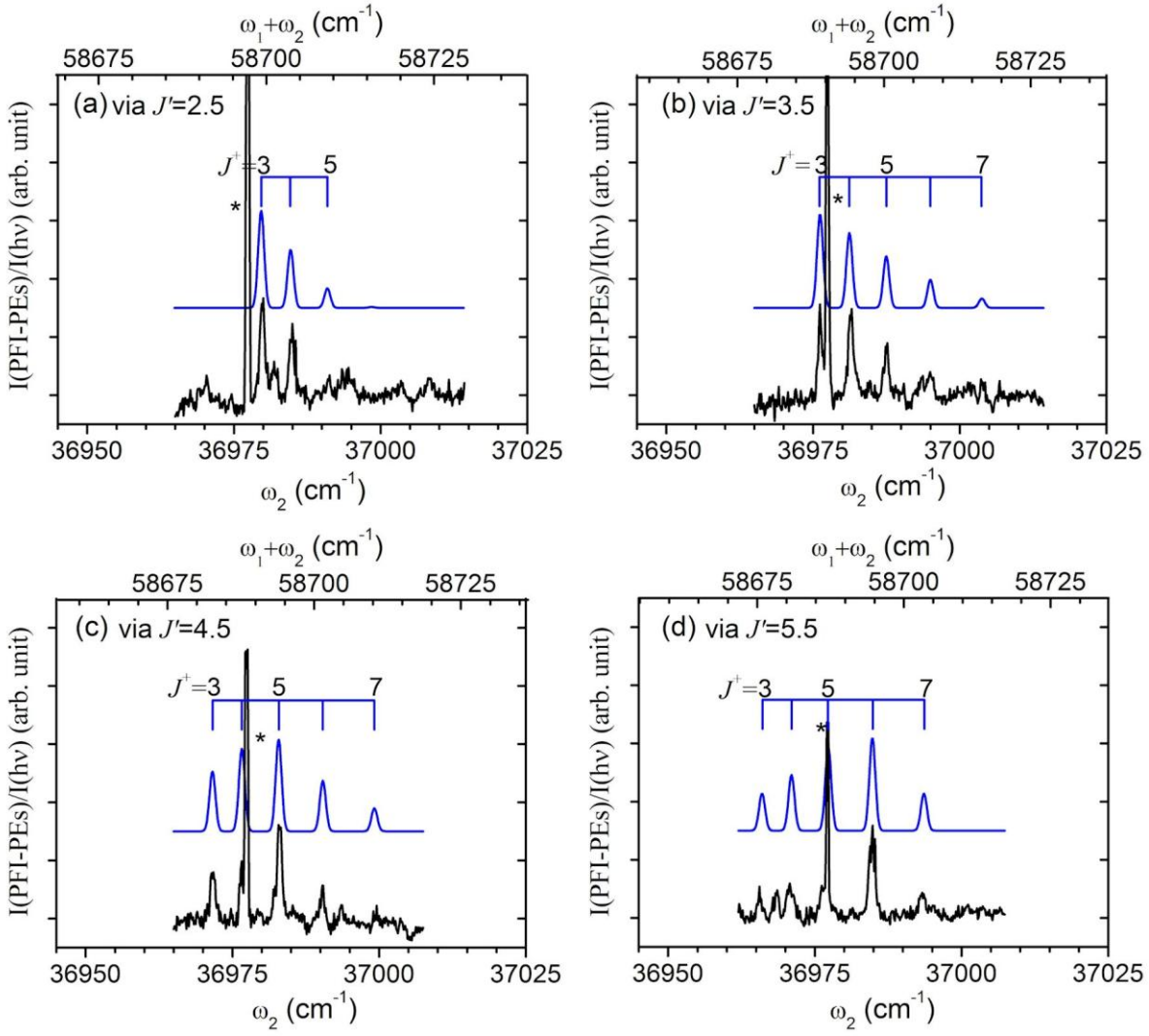

Figure 9

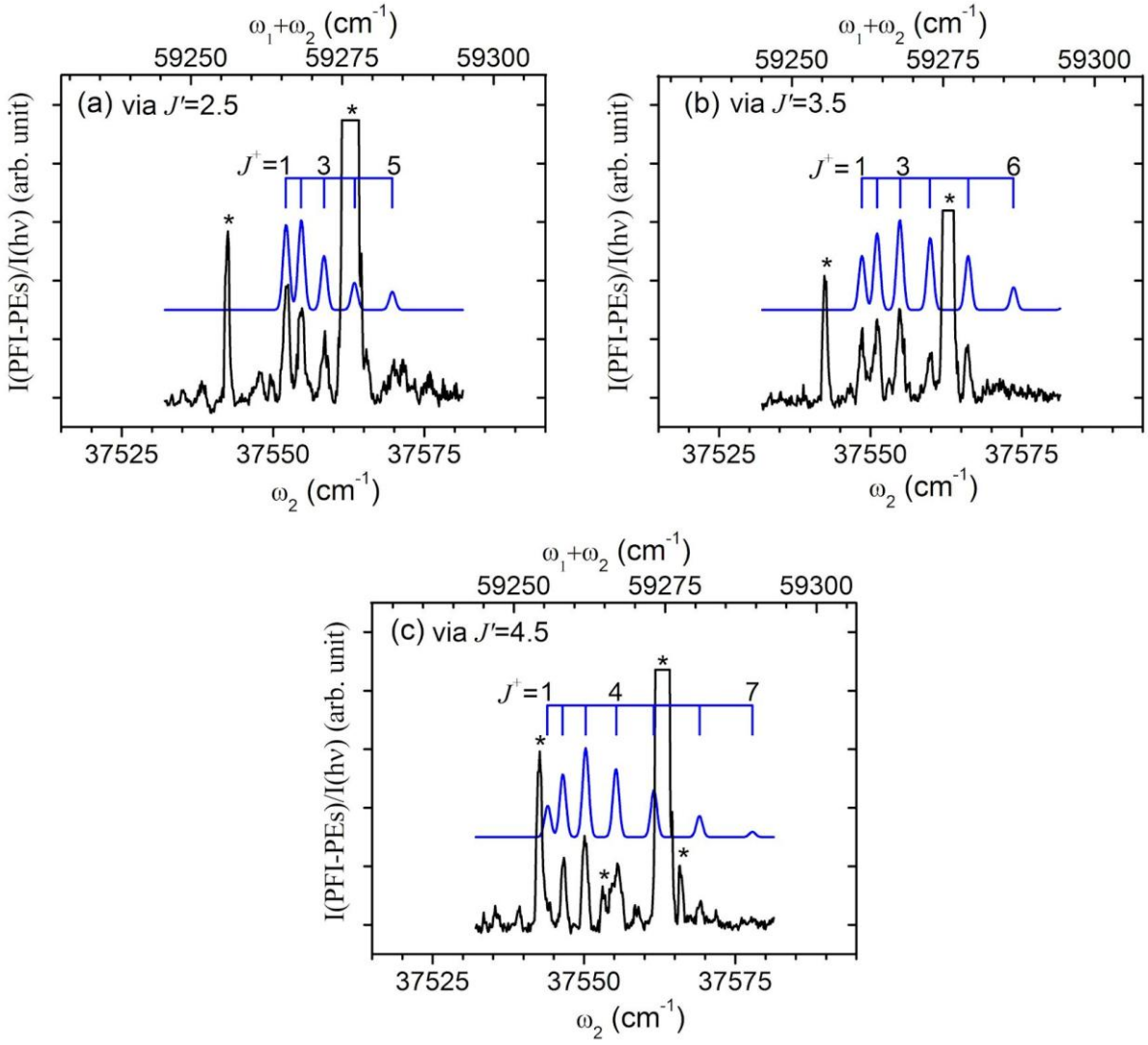

Figure 10

TABLE I. Energetic and spectroscopic data of obtained by PFI-PE study of VC^+.

Note	Parameter	Unit	$VC^+(X^3\Delta_1, v^+)^a$	$VC^+(X^3\Delta_2, v^+)^a$	$VC^+(X^3\Delta_3, v^+)^a$	Other works
Ionization energy	IE[b]	eV	7.13058±0.00010			7.36[c]
		cm^{-1}	57512.0±0.8			
$v^+=0$	ν_{00}^+	cm^{-1}	57512.3±0.8	57656.2±0.8	57813.2±0.8	
	B_0^+	cm^{-1}	0.6330±0.0010	0.6479±0.0042	0.6330±0.0020	
$v^+=1$	ν_{10}^+	cm^{-1}	58397.5±0.8	58540.5±0.8	58697.6±0.8	
	B_1^+	cm^{-1}	0.6272±0.0007	0.6323±0.0012	0.6270±0.0012	
$v^+=2$	ν_{20}^+	cm^{-1}	59271.3±0.8			
	B_2^+	cm^{-1}	0.6264±0.0023			
Vibrational constants	ΔG(1/2)	cm^{-1}	885.1±0.8	884.3±0.8	884.4±0.8	
	ΔG(3/2)	cm^{-1}	873.8±0.8			
	ω_e^+	cm^{-1}	896.43±0.8			874[d]
	$\omega_e^+ x_e^+$	cm^{-1}	5.7±0.8			8.8[d]
Rotational constants	B_e^+	cm^{-1}	0.6338±0.0025			
	α_e^+	cm^{-1}	0.0033±0.0007			
Equilibrium bond length	r_e^+	Å	1.6549±0.0003			1.667[d]
Spin-orbit constant	A	cm^{-1}	75.2±0.8			
0 K bond energy difference	$D_0(V^+–C)$ $–D_0(V–C)$	cm^{-1}	–0.38425±0.00012			–0.47±0.29[e] –0.39 ± 0.25[f]

[a] This work.

[b] Iobization energy is defined as energy seperation between $VC^+(X^3\Delta_1, v^+=0, J^+=1)$ cationic state and $VC(X^2\Delta_{3/2}, v^+=0, J''=3/2)$ neutral state.

[c] Theoretical prediction (Ref.13).

[d] Theoretical predictions (Ref.14).

[e] Derived from experimental D_0(V-C) (Ref. 51) and $D_0(V^+$-C) (Ref. 15).

[f] Derived from experimental D_0(V-C) (Ref. 51) and $D_0(V^+$-C) (Ref. 16).

[g] The uncertainities of B_0^+, B_1^+, B_2^+, B_e^+ and α_e^+ are ±σ (σ: standard deviation is resulting from least square fits).

[h] The uncertainities of ν_{00}^+, ν_{10}^+, ν_{20}^+, ΔG(1/2), ΔG(3/2), ω_e^+, $\omega_e^+ x_e^+$ are due to pulsed field ionization.

Table II. The bond length r_e (r_e^+) in Å and harmonic vibrational frequency ω_e (ω_e^+) in cm^{-1} for $VC(X^2\Delta)/VC^+(X^3\Delta)$ predicted at the CCSD(T), CCSDT, CCSDTQ, MRCI+Q, and B3LYP using aug-cc-p(wC)VXZ levels, where X = T, Q and 5.

	$VC(^2\Delta)$		$VC^+(^3\Delta)$	
	r_e	ω_e	r_e^+	ω_e^+
CCSD(T)/aug-cc-pVTZ	1.629	811	1.652	935
CCSD(T)/aug-cc-pVQZ	1.621	842	1.646	949
CCSD(T)/aug-cc-pV5Z	1.619	851	1.645	953
CCSD(T)/aug-cc-pwCVTZ[a]	1.605	871	1.631	993
CCSD(T)/aug-cc-pwCVQZ[a]	1.598	892	1.626	1019
CCSD(T)/aug-cc-pwCV5Z[a]	1.595	902	1.624	1030
CCSDT/aug-cc-pVTZ	1.619	916	1.653	926
CCSDTQ/cc-pVTZ	1.626	911	1.666	878
MRCI	1.636[b]	/	1.667[c]	874[c]
MRCI+Q/aug-cc-pwCVTZ[a]	1.611	925	1.654	886
B3LYP/aug-cc-pVTZ	1.581	946	1.606	980
Expt.			1.6549	896.4
			± 0.0003	± 0.8

[a] Correlated with the *3s3p3d4s* (V) and *1s2s2p* (C) electrons.

[b] Ref. 12.

[c] Ref. 14.

Table III. Individual energy contributions to the CCSDTQ/CBS predictions for the IE(VC), IE(V), D_0(V–C), and $D_0(V^+–C)$ values. [a]

		IE(VC)	IE(V)	D_0(V–C)	$D_0(V^+–C)$	$D_0(V^+–C) – D_0$(V–C)
$\Delta E_{\text{extrapolated CBS}}$ [b]	Eq. (1)	7.157	6.463	4.164	3.470	–0.694
	Eq. (2)	7.167	6.455	4.198	3.486	–0.712
	Average	7.162	6.459	4.181	3.478	–0.703
ΔE_{CV} [c]	(T)→T	0.023	–0.001	0.037	0.013	–0.024
ΔE_{ZPVE} [d]		–0.002	/	–0.056	–0.054	0.002
ΔE_{SO} [e]		–0.002	0.014	–0.027	–0.011	0.016
ΔE_{SR} [f]	CCSD(T)	–0.015	0.275	–0.150	0.140	0.290
	(T)→T	0.002	0.000	0.004	0.002	–0.002
	T→Q	0.002	0.000	–0.001	–0.003	–0.002
	Subtotal	–0.011	0.275	–0.147	0.139	0.286
ΔE_{HOC} [g]	(T)→T	–0.019	0.016	–0.090	–0.055	0.035
	T→Q	–0.025	0.003	0.125	0.153	0.028
	Subtotal	–0.044	0.019	0.035	0.098	0.063
CCSDTQ/CBS [h]		7.126	6.766	4.023	3.663	–0.360
Expt.		7.13058 ±0.00010 [i]	6.74633 ± 0.00012 [j]	4.34 ±0.25 [k]	3.87 ±0.14 [l] 3.95 ±0.04 [m]	–0.38425 ±0.00012 [i]

[a] All quantities and energy differences are in eV.

[b] Extrapolated from the CCSD(T) energies using Eqs. (1) and (2), respectively.

[c] Core-valence electronic correlation obtained as the energy difference between CCSD(T) and CCSDT levels using the aug-cc-pwCVTZ basis set.

[d] Based on the harmonic vibrational frequencies at the CCSDTQ/cc-pVTZ level.

[e] Spin-orbit coupling obtained at the MRCI level with the uncontracted aug-cc-pVTZ basis set.

[f] Scalar relativistic effect calculated at the CCSD(T)/aug-cc-pV5Z–DK, CCSDT/aug-cc-pVQZ–DK and CCSDTQ/cc-pVTZ–DK levels.

[g] Higher-order effect calculated at the CCSDT/aug-cc-pVQZ and CCSDTQ/cc-pVTZ levels.

[h] IE or $D_0 = \Delta E_{\text{extrapolated CBS}} + \Delta E_{CV} + \Delta E_{ZPVE} + \Delta E_{SO} + \Delta E_{SR} + \Delta E_{HOC}$.

[i] This work.

[j] From Ref. 28.

[k] From Ref. 51.

[l] From Ref. 15.

[m] From Ref. 16.

Table IV. Individual energy contributions to the CCSDTQ/CBS atomization energies, ΔH^{o}_{f0} and ΔH^{o}_{f298} values for VC/VC^{+}. [a]

		VC	VC^{+}
$\Delta E_{extrapolatedCBS}$ [b]	Eq. (1)	401.8	−288.7
	Eq. (2)	405.0	−286.5
	Average	403.4	−287.6
ΔE_{CV} [c]	(T)→T	3.6	1.4
ΔE_{ZPVE}		−5.4	−5.2
ΔE_{SO} [d]		−2.6	−2.4
ΔE_{SR} [e]	CCSD(T)	−14.5	−13.0
	(T)→T	0.4	0.2
	T→Q	−0.1	−0.3
	Subtotal	−14.2	−13.1
ΔE_{HOC} [f]	(T)→T	−8.7	−6.9
	T→Q	12.1	14.5
	Subtotal	3.4	7.6
CCSDTQ/CBS $\sum D_0$ [g]		388.2	−299.4
CCSDTQ/CBS ΔH^{o}_{f0} [h]		835.2	1522.8
CCSDTQ/CBS ΔH^{o}_{f298} [i]		840.4	1528.0
Expt. ΔH^{o}_{f0}		≈804 ± 24 [j]	≈1492 ± 24 [j]
		812.9 ± 14 [k]	1500.9 ± 14 [k]
		805.2 ± 4 [l]	1493.2 ± 4 [l]
Expt. ΔH^{o}_{f298}		≈809 ± 24 [j]	≈1497 ± 24 [j]
		818.1 ± 14 [k]	1506.1 ± 14 [k]
		810.4 ± 4 [l]	1498.4 ± 4 [l]

[a] All quantities and energy differences are in kJ mol^{-1}.

[b] Extrpolated from the CCSD(T) energies using Eqs. (1) and (2), respectively.

[c] Core-valence electronic correlation obtained as the energy difference between CCSD(T) and CCSDT levels using the cc-pwCVTZ basis set.

[d] Spin-orbit coupling obtained at the MRCI level with the uncontracted aug-cc-pVTZ level.

[e] Scalar relativistic effect calculated at the CCSD(T)/aug-cc-pV5Z-DK, CCSDT/aug-cc-pVQZ-DK, and CCSDTQ/cc-pVTZ-DK levels.

[f] Higher-order effect calculated at the CCSDT/aug-cc-pVQZ and CCSDTQ/cc-pVTZ levels.

[g] $\sum D_0 = \Delta E_{\text{extrapolated CBS}} + \Delta E_{CV} + \Delta E_{ZPVE} + \Delta E_{SO} + \Delta E_{SR} + \Delta E_{HOC}$.

[h] $\Delta H^{o}_{f0} = \Delta H^{o}_{f0}(V) + \Delta H^{o}_{f0}(C) - \sum D_0$.

[i] $\Delta H^{o}_{f298} = \Delta H^{o}_{f298}(V) + \Delta H^{o}_{f298}(C) - \sum D_0$ − thermal and enthalpy corrections.

[j] Deduced from $D_0(V-C) = 419 \pm 24$ kJ mol^{-1} (Ref. 51), IE(VC) = 7.13058 ± 0.00010 eV, $\Delta H^{o}_{f0}(V) = 512.2$, and $\Delta H^{o}_{f0}(C) = 711.2$ kJ mol^{-1} (Ref. 48), all values are rounded up to no decimal place.

[k] Deduced from $D_0(V^{+}-C) = 3.87 \pm 0.14$ eV (Ref. 15), IE(VC), $\Delta H^{o}_{f0}(V^{+})$, and $\Delta H^{o}_{f0}(C)$.

[l] Deduced from $D_0(V^{+}-C) = 3.95 \pm 0.04$ eV (Ref. 16), IE(VC), $\Delta H^{o}_{f0}(V^{+})$, and $\Delta H^{o}_{f0}(C)$.